JCI The Journal of Clinical Investigation

FOXA1 overexpression suppresses interferon signaling and immune response in cancer

Yundong He, … , Shancheng Ren, Haojie Huang

J Clin Invest. 2021. https://doi.org/10.1172/JCI147025.

Research In-Press Preview Cell biology

Graphical abstract

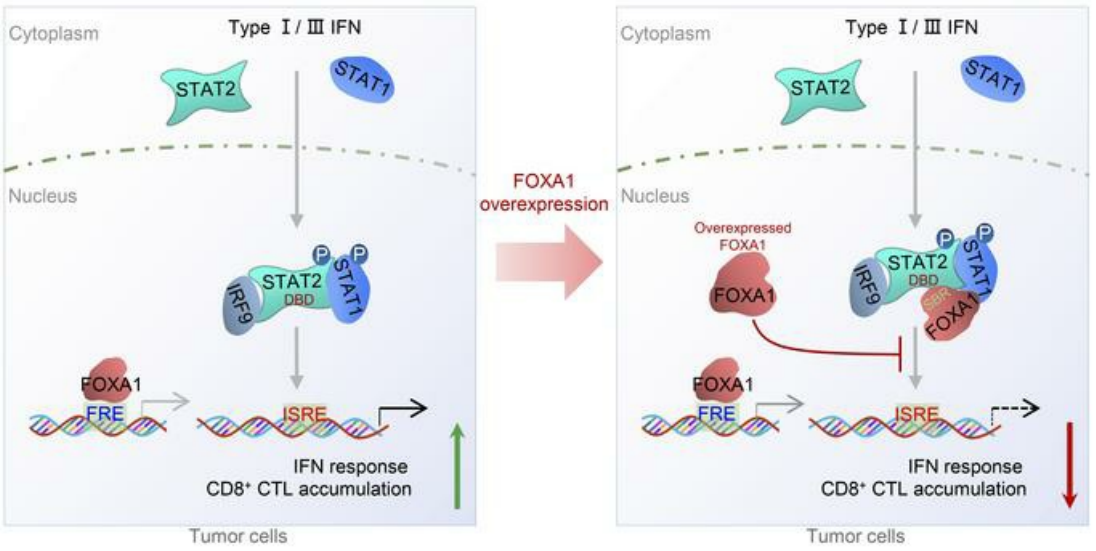

FOXA1 overexpression suppresses interferon signaling and immune response in cancer

Yundong He[1,2], Liguo Wang[3], Ting Wei[3], Yu-Tian Xiao[4], Haoyue Sheng[1,5,6], Hengchuan Su[5,6], Daniel P. Hollern[7], Xiaoling Zhang[8], Jian Ma[1,5,6], Simeng Wen[1], Hongyan Xie[1], Yuqian Yan[1], Yunqian Pan[1], Xiaonan Hou[9], Xiaojia Tang[3], Vera J. Suman[3], Jodi M. Carter[10], Richard Weinshilboum[11], Liewei Wang[11], Krishna R. Kalari[3], Saravut J. Weroha[9], Alan H. Bryce[12], Judy C. Boughey[13], Haidong Dong[2,14], Charles M. Perou[7], Dingwei Ye[5,6], Matthew P. Goetz[9,15], Shancheng Ren[4]* and Haojie Huang[1,2,15]*

[1]Department of Biochemistry and Molecular Biology, Mayo Clinic College of Medicine and Science, MN 55905, USA

[2]Department of Urology, Mayo Clinic College of Medicine and Science, Rochester, MN 55905, USA

[3]Division of Computational Biology, Mayo Clinic College of Medicine and Science, Rochester, MN 55905, USA

[4]Department of Urology, Shanghai Changhai Hospital, Shanghai 200433, China

[5]Department of Urology, Fudan University Shanghai Cancer Center, Shanghai 200032, China

[6]Department of Oncology, Shanghai Medical College, Fudan University, Shanghai 200032, China

[7]Lineberger Comprehensive Cancer Center, University of North Carolina, Chapel Hill, NC 27599, USA

[8]Key Laboratory of Organ Regeneration and Transplatation of the Ministry of Education, Institute of Immunology, The First Hospital of Jinlin University, Changchun, Jilin 130021, China

[9]Department of Oncology, Mayo Clinic College of Medicine and Science, Rochester, MN 55905, USA

[10]Department of Laboratory Medicine and Pathology, Mayo Clinic College of Medicine and Science, Rochester, MN 55905, USA

[11]Department of Molecular Pharmacology and Experimental Therapeutics, Mayo Clinic College of Medicine and Science, Rochester, MN 55905, USA

[12]Division of Hematology and Oncology, Department of Internal Medicine, Mayo Clinic College of Medicine and Science, Phoenix, AZ 85054, USA

[13]Department of Surgery, Mayo Clinic College of Medicine and Science, Rochester, MN 55905, USA

[14]Department of Immunology, Mayo Clinic College of Medicine and Science, Rochester, MN 55905, USA

[15]Mayo Clinic Cancer Center, Mayo Clinic College of Medicine and Science, MN 55905, USA

*** Corresponding Author**: Haojie Huang or Shencheng Ren.

Address correspondence to: Haojie Huang, 200 First Street SW, Rochester, MN 55905, USA; Phone: 507.293.1311; E-mail: huang.haojie@mayo.edu. Or: Shencheng Ren, 168 Changhai Road, Shanghai 200433, China; Phone: 021.311.617.18; E-mail: renshancheng@gmail.com.

Abstract

Androgen receptor (AR)-positive prostate cancers (PCa) and estrogen receptor (ER)-positive luminal breast cancers (BCa) are generally less responsive to immunotherapy compared to certain tumor types such as melanoma. However, the underlying mechanisms are not fully elucidated. Here we found that FOXA1 overexpression inversely correlated with interferon (IFN) signature and antigen presentation gene expression in PCa and BCa patients. FOXA1 bound STAT2 DNA binding domain and suppressed STAT2 DNA binding activity, IFN signaling gene expression and cancer immune response independently of the transactivation activity of FOXA1 and its mutations detected in prostate and breast cancers. Increased FOXA1 expression promoted cancer immuno- and chemotherapy resistance in mice and PCa and BCa patients. These findings were also validated in bladder cancer expressing high level FOXA1. FOXA1 overexpression could be a prognostic factor to predict therapy resistance and a viable target to sensitize luminal prostate, breast and bladder cancer to immuno- and chemotherapy.

Introduction

Patients with certain cancer types such as melanoma and non-small cell lung cancer have significantly benefited from immunotherapies such as immune checkpoint inhibitors (ICIs) (1). However, ICIs including the cytotoxic T lymphocyte antigen 4 (CTLA4) antibody ipilimumab and anti-PD-1 antibody pembrolizumab exhibit limited anticancer activity in PCa, most of which are AR-positive (AR^+) (2). Similarly, BCa, especially the ER-positive (ER^+) subtype, also exhibits very limited response to immunotherapy (3). Thus, AR^+ PCa and ER^+ BCa are generally considered as immunologically "cold" cancer types and it is of paramount importance to decipher the underlying mechanisms which drive resistance to immunotherapy. One factor underlying immunologically "cold" PCa and BCa relates to low levels of tumor mutation burden (TMB). Surprisingly, some studies suggest that the ICI therapy response is not significantly associated with TMB in BCa and melanoma (4, 5) while others show that upregulation of interferon γ (IFNγ) response pathway genes are associated with improved clinical responses to ICI in PCa with low TMB (6).

Activation of signaling pathways in tumor in response to IFNs including type I (such as IFNα and IFNβ), type II (IFNγ) and type III IFN (such as IFNλs) is essential for cytotoxic T lymphocyte (CTL)-mediated killing of cancer cells (7-12). High expression of IFN signaling genes is associated with greater response to ICIs in melanoma and neck squamous cell carcinoma (13). IFN exposure of cancer cells induces expression of IFN-stimulated genes (ISGs) including antigen presentation machinery (APM) genes such as major histocompatibility complex class I (MHC I) (14). Presentation of cancer-specific neoantigens, which is regulated by IFN signaling, is a key factor affecting cytotoxic T (Tc) cell activity and ICI therapy efficacy (15-17). This critical step is governed by MHC or human leukocyte antigen (HLA) that presents intra-cellular

peptides on cell surface recognized by the T cell receptor (TCR). As a result, this immune-stimulating signaling cascade triggers infiltration of CTLs, mainly Tc and natural killer (NK) cells, ultimately leading to granule exocytosis as a common mechanism to destroy cancer cells by expressing and releasing the pore forming proteins including perforin 1 (PRF1), granule-associated enzymes or termed granzymes (GZMs) and NK cell granule protein 7 (NKG7).

Improved clinical outcomes have been achieved for certain cancer types such as melanoma after treatment with immunotherapies including adoptive transfer of tumor-infiltrating lymphocytes (TILs) and application of ICIs (e.g. CTLA4, PD1, and PD-L1 blockade antibodies) (18-21). However, disease relapse often occurs after initial tumor regression and becomes immunotherapy resistant. Notably, as demonstrated in melanoma, such resistance has been linked to the genetic alterations such as mutations and somatic copy number alterations in IFN/receptor signaling and APM genes (7, 18, 22, 23).

The transcription factor FOXA1 is a well-studied pioneer factor required for AR and ER activities in PCa and BCa cells (24-26). *FOXA1* gene is also implicated in these two cancer types due to its frequent mutations (27-30). The frequency of somatic point mutations of FOXA1 is around 4-8% and FOXA1 mutations promote cancer progression by reprogramming the functions of AR and other factors in these cancer types (27-31). In the present study, we identified a new role of FOXA1 in suppressing IFN signaling and cancer immune response which drives cancer immune evasion and therapy resistance. Importantly, this novel function is independent of the well-known pioneer factor function of FOXA1 and its mutations detected in PCa and BCa.

Results

FOXA1 inversely correlates with IFN signaling activity in PCa and BCa. The "immune coldness" commonly observed in a few cancer types such as AR^+ PCa and ER^+ luminal BCa prompted us to hypothesize that there might be a common immune evasion mechanism shared by different cancers. As demonstrated in melanoma, low IFN activation predicts unfavorable prognosis of ICI immunotherapy (Supplementary Figure 1A) and deletion of IFN pathway genes links to ICI resistance (5, 7, 13), suggesting that inactivation of IFN pathway may confer to immune evasion in cancers. We demonstrated that expression signature of IFN response genes (termed IFN activity or score) in the TCGA cohort of PCa and luminal BCa was significantly lower than that in melanoma, lung and kidney cancers which are generally responsive to ICIs (32-34) (Supplementary Figure 1B). Therefore, we performed meta-analysis of the TCGA PCa and BCa RNA-seq datasets to search for genes that are negatively correlated with IFN activity. We demonstrated that *FOXA1* is the only common gene among the top 5 hits, the expression of which negatively correlated with IFN activity in both PCa and BCa cohorts (Supplementary Figure 1C). Gene Set Enrichment Analysis (GSEA) also revealed a negative correlation between expression of *FOXA1* and IFN response genes in TCGA cohorts of PCa and BCa patients (Figure 1A). To corroborate the meta-analysis data, we performed single cell RNA sequencing (scRNA-seq) in PCa patient samples and demonstrated that *FOXA1* level was inversely associated with expression of IFN response signature genes and APM genes in luminal cell population (Figure 1B; Supplementary Figure 1D; Supplementary Table 1; Supplementary Table 2). Similar results were obtained from BCa cells through meta-analysis of scRNA-seq data from two cohorts of BCa patient specimens (35, 36) (Figure 1C). These findings are consistent with the results obtained from the analysis of RNA-seq data from bulk tissues in different cohorts with primary and metastatic PCa and BCa, respectively (Supplementary Figure 2). Aberrant activation of IFN

signaling genes in FOXA1-low tumors in both TCGA PCa and BCa cohorts was unlikely caused by either genomic alterations in IFN response genes or overall TMB because there was no obvious correlation between *FOXA1* expression and genomic alterations in IFN response genes or overall TMB (Supplementary Figure 3). *FOXA1* mRNA level was highly upregulated but intriguingly, *CD274* (PD-L1) mRNA expression was downregulated in PCa and BCa tissues compared with normal tissues in various cohorts examined (Supplementary Figure 4). Together, our data indicate that overexpression of FOXA1 may play a pivotal role in regulating "immune coldness" by modulating IFN response gene expression in PCa and BCa.

FOXA1 binds the DNA binding domain (DBD) and inhibits DNA binding ability of STAT2. To explore possible molecular mechanisms underlying FOXA1 inhibition of IFN signaling, we first examined the co-localization of FOXA1 with STAT1 and STAT2, two major effectors of IFN signaling. FOXA1 protein was primarily detected in the nucleus in LNCaP cells regardless of IFNα treatment (Figure 2A). STAT1 protein was localized in both cytoplasm and nucleus while STAT2 was mainly localized in the cytoplasm of LNCaP cells grown in regular medium without additional IFNα stimulation (Figure 2A). IFNα treatment increased localization of both STAT1 and STAT2 proteins in the nucleus where they were co-localized with FOXA1 (Figure 2A). Since phosphorylation of STAT1/2 is important for their nuclear localization, we sought to determine whether FOXA1 affects STAT1/2 phosphorylation. We found that neither ectopic expression of FOXA1 in FOXA1-negative cell lines such as DU145 and MDA-MB-231 nor knockdown (KD) of endogenous FOXA1 in LNCaP and MCF7 cell lines had any effect on STAT1 and STAT2 protein phosphorylation (Supplementary Figure 5, A-D). Consistent with nuclear localization status of FOXA1 (Figure 2A), co-immunoprecipitation (co-IP) assay showed

that FOXA1 interacted with STAT1 and STAT2 at endogenous level in the nucleus of LNCaP and MCF7 cells treated with IFNα (Figure 2B). Similarly, we observed that FOXA1 binds to STAT1 in the nucleus in both cell lines stimulated with IFNγ although STAT1 homodimer association with FOXA1 was much weaker than STAT1/STAT2 heterodimer (Figure 2B), and this result was confirmed by reciprocal co-IP experiments (Figure 2C). FOXA1 overexpression also had no effect on STAT2/STAT1/IRF9 and STAT1/STAT1 complex formation following the stimulation of IFNα and IFNγ, respectively (Supplementary Figure 5E). These data suggest that FOXA1 expression does not affect the formation of STAT1 and/or STAT2 protein-containing complex in cells stimulated with type I or II IFNs.

Since binding of FOXA1 with STAT2/STAT1 in IFNα-stimulated cells was much stronger than that to STAT1/STAT1 in IFNγ-treated cells (Figure 2, B and C), we chose to further characterize how FOXA1 binds to STAT2. Co-IP assays using two STAT2 N-terminal truncation mutants indicated that FOXA1 binds STAT2 DBD (Supplementary Figure 5F). Glutathione S-transferase (GST) pulldown assay confirmed that FOXA1 directly bound STAT2-DBD in vitro (Supplementary Figure 5G). We further performed in vitro protein binding assay using different GST-STAT2 DBD truncation mutants and demonstrated that FOXA1 bound more than two thirds (a.a. 366-486) of STAT2 DBD (a.a. 312-486) (Supplementary Figure 5H).

We also determined which region in FOXA1 interacts with STAT2. Mutagenesis and GST pulldown assays showed that the middle portion of FOXA1 (FOXA1-M, a.a. 141-294), which contains the forkhead domain (FKHD, a.a. 168-269), bound STAT2 DBD (Supplementary Figure 5I). We further generated three additional C-terminal truncation mutants from FOXA1-M (Figure 2D) and utilized them for GST pulldown and co-IP assays. We found that deletion of the C-terminal portion of FOXA1-M (a.a. 247-294) abolished FOXA1 interaction with STAT2 DBD

and this fragment is termed as the STAT2 binding region (SBR) of FOXA1 (Figure 2, D and E; Supplementary Figure 5J). The protein binding results were fully supported by the data obtained from IFN-sensitive response element (ISRE)-based luciferase reporter gene assay (Supplementary Figure 5K). These findings suggest that the SBR is required for FOXA1 binding of STAT2 and suppression of IFN activity.

Since the SBR contains the Wing2 motif (a.a. 247-269), a key region involved in regulating the DNA binding activity of FOXA1 DBD (29, 30, 37) (Figure 2D), we sought to determine whether DNA binding ability of FOXA1 is required for inhibition of IFN signaling. The α-helix 3 (αH3, a.a. 212-225), especially residues N216, H220 and N225 in the FKHD domain of FOXA1 have direct contact with DNA (37). We generated two DNA binding-deficient mutants FOXA1-N216A/H220A/N225A (FOXA1-αH3m) and FOXA1Δ212-225 (FOXA1ΔαH3) by mutating these three residues to alanine and deleting the entire αH3, respectively. Results from electrophoretic mobility shift assay (EMSA) and luciferase reporter assay confirmed that these mutants lost their ability to bind to the cognate FOXA1-response DNA element (FRE) in the *KLK3* (PSA) gene enhancer and to initiate FOXA1 gene transactivation activity (29, 30) (Supplementary Figure 5, L and M). However, apart from the FOXA1ΔSBR mutant, these two DNA-binding deficient mutants of FOXA1 were still able to bind STAT2 DBD and inhibit IFN activity (Figure 2, F and G), suggesting that FOXA1 suppresses IFN signaling independently of its DNA binding function. We further performed biotin pulldown assay using biotin-labeled ISRE DNA oligo (biotin-ISRE) (Supplementary Figure 5N, top). We demonstrated that addition of in vitro generated FOXA1-WT and FOXA1ΔαH3 mutant (deletion of DNA contacting region) proteins prohibited STAT2 binding of its targeting DNA sequence ISRE in the nuclear extract of IFNα-stimulated FOXA1-negative DU145 cells (Supplementary Figure 5N, bottom). However,

this role of FOXA1 was abolished by deletion of the SBR (FOXA1ΔSBR) (Supplementary Figure 5N, bottom). Moreover, no FOXA1 protein was pulled down by the biotin-labeled ISRE DNA oligo, but rather FOXA1 bound STAT2 in a dose-dependent manner in the chromatin-free fraction of the nuclear extract (Supplementary Figure 5N, bottom). These data suggest that high level FOXA1 inhibits the ability of STAT2 to bind to its target DNA sequence (ISRE). This notion is further supported by the results from EMSA assay that STAT2 binding of the ISRE probe was inhibited in lysate of DU145 cells transfected with FOXA1-WT and FOXA1ΔαH3 mutant, but no such effect was observed for FOXA1ΔSBR mutant or AR (Supplementary Figure 5O). Together, these data indicate that FOXA1 inhibits STAT2 DNA binding ability and this new function of FOXA1 does not rely on its DNA binding ability.

FOXA1 impedes IFNα-induced STAT2 chromatin occupancy and the effect is independent of its mutations in cancer. Next, we sought to determine whether FOXA1 affects STAT2 genome-wide binding on chromatin. We first knocked down the endogenous FOXA1 in FOXA1-high LNCaP cells with small interfering RNA (siRNA) specifically targeting 3' untranslated region (3'UTR) and then rescued with siRNA-non-targetable FOXA1-WT, DNA binding-deficient mutant FOXA1ΔαH3 or STAT2 binding deficient mutant FOXA1ΔSBR (Supplementary Figure 6A). These FOXA1 expression-manipulated cell lines were utilized for STAT2 chromatin-immunoprecipitation sequencing (ChIP-seq) analysis. The ChIP-seq replicates in each cellular condition were well correlated (Supplementary Figure 6B). We identified totally 794 STAT2 binding peaks, including 192 significantly upregulated peaks (termed Up-peaks), 45 downregulated peaks (termed Down-peaks) and 557 peaks with no significantly alterations (termed NSA-peaks) following FOXA1 KD (Figure 3, A and B; Supplementary Figure 6, C and

D). The Up-peaks tend to distribute towards gene promoters whereas the NSA-peaks and Down-peaks appear to go to opposite directions (Supplementary Figure 6E). MEME-ChIP motif analysis revealed that the STAT2 motif was the top hit among the Up-peaks, but no such enrichment was observed in the NSA-peaks and Down-peaks (Figure 3C). Gene ontology biological process (GO-BP) analysis revealed that the genes associated with FOXA1 KD-induced Up-peaks were highly related to STAT2 relevant pathways (such as IFN and immune responses), but no such enrichment was observed in the NSA-peaks and Down-peaks (Supplementary Figure 6F).

IFNα-stimulated and FOXA1 KD-enhanced STAT2 binding on chromatin was confirmed at the canonical IFN signaling gene loci such as *ISG15*, *IFI44*, *HLA-E* and *PSMB9* (Supplementary Figure 7A). These results were further validated by ChIP-qPCR data in both LNCaP and MCF7 cell lines (Figure 3D; Supplementary Figure 7B). Restored expression of both FOXA1 WT and FOXA1ΔαH3 but not FOXA1ΔSBR reversed FOXA1 KD-enhanced STAT2 binding at target loci (Figure 3D; Supplementary Figure 7A). These results support the notion that FOXA1 suppresses STAT2 chromatin binding and IFN signaling in a manner dependent on FOXA1 binding of STAT2, but this effect does not require the DNA binding activity of FOXA1.

Different from the FOXA1 impact on STAT2 occupancy on chromatin, IFNα treatment had little or no effect on genome-wide chromatin engagement of FOXA1 in LNCaP cells (Supplementary Figure 8A). Less than 0.5% of total FOXA1 peaks overlapped with STAT2 binding peaks identified in LNCaP cells (Supplementary Figure 7A; Supplementary Figure 8B). FOXA1 impact on STAT2 chromatin occupancy but not vice versa could be explained, at least in part by the observation that the abundance of *STAT2* mRNA was significantly lower compared to *FOXA1* mRNA in LNCaP and PCa patient samples (Supplementary Figure 8C).

These results support a model wherein FOXA1 forms a protein complex with STAT2 and inhibits STAT2 occupancy at its target gene loci containing STAT2 DNA binding motif, but has no obvious effect on loci without such motif. This model is consistent with the finding from the biotin-labeled ISRE pulldown assay that FOXA1 inhibits STAT2 DNA binding ability and has no association with STAT2 DNA binding motif (Supplementary Figure 5N). This model is also supported by the observation that STAT2 binding peaks containing STAT2 DNA binding motif (Up-peaks) had very minimal ($\leqslant$ 5%) overlap with FOXA1 binding peaks identified LNCaP and PCa patient samples (38) (Supplementary Figure 8D). These results support the working model that FOXA1 binds to the DNA binding domain of STAT2, thereby blocking STAT2 binding of the canonical STAT2 DNA binding motif, but not other motifs indirectly associated with STAT2 (Supplementary Figure 8E).

FOXA1 suppression of STAT2 occupancy on chromatin is independent of its mutations in cancer. *FOXA1* gene is frequently mutated in hormone-receptor-driven cancers such as PCa and BCa (27-30). FOXA1 mutations reprogram its pioneer factor activity and enhance PCa aggressiveness (29, 30). We first investigated whether cancer-associated FOXA1 missense mutations affect STAT2 function and IFN activity. We found that PCa-derived "hotspot" missense mutants of FOXA1, including FOXA1-H247Q, FOXA1-R261G, and FOXA1-F266L, were able to bind STAT2 to an extent similar to FOXA1 WT (Supplementary Figure 9A). Using R261G, one of the 'hotspot' mutants as a working model, STAT2 ChIP-seq data revealed that restored expression of FOXA1-R261G completely reversed FOXA1 depletion-enhanced STAT2 occupancy on chromatin in IFNα-treated LNCaP cells, an effect similar to FOXA1 WT (Figure 3B; Supplementary Figure 7A). We also confirmed that similar to FOXA1 WT, restored

expression of PCa-derived mutants FOXA1-H247Q and FOXA1-R261G revered FOXA1 KD-enhanced expression of IFN signaling pathway proteins such as ISG15 and MHC I in both LNCaP and VCaP PCa cell lines (Supplementary Figure 9, B and C). We further verified the STAT2-inhibitory effect of these cancer-associated FOXA1 mutants using ISRE-based luciferase reporter assays (Supplementary Figure 9D). Moreover, there was no significant difference in expression of IFN response and APM genes between FOXA1 WT and mutated prostate and breast tumors in TCGA cohorts (Supplementary Figure 9E). Collectively, these data suggest that the PCa-derived FOXA1 misense mutants, at least those "hotspot" mutants we examined, remain the ability to inhibit STAT2 chromatin occupancy, IFN activity and cancer immune response gene expression. While a significant fraction of FOXA1 mutations in cancer are C-terminal truncation mutations (29, 30), we demonstrated that different from the SBR-deficient mutant FOXA1 (1-247), the two PCa-associated C-terminal truncation mutants FOXA1 (1-290) and FOXA1 (1-268) (29, 30) remained the ability to bind to STAT2 and suppress IFN-induced STAT2 transcriptional activity (Supplementary Figure 9, F-H), suggesting that STAT2 inhibitory effect of FOXA1 is also not affected by FOXA1 C-terminal truncation mutations.

Identification of FOXA1-affected STAT2 target genes via transcriptome analysis. We globally assessed the impact of FOXA1 on STAT2 target gene expression at transcriptional level. We knocked down FOXA1 in LNCaP cells in the presence or absence of IFNα treatment and harvested these cells for RNA-seq analysis. The replicates of RNA-seq data correlated very well (Supplementary Figure 10A). Through unsupervised cluster analysis of differentially expressed genes, we identified a subset of IFNα-stimulated genes (n = 172), expression of which were significantly increased after FOXA1 KD (Supplementary Figure 10B). We further performed

integrated analysis of STAT2 ChIP-seq and RNA-seq data and identified 62 FOXA1-suppressed STAT2 target genes (Figure 4A). GO-BP analysis revealed that this set of genes were strongly relevant to IFN or immune responses (Figure 4B). Importantly, we found that FOXA1 KD induced upregulation of this set of genes in LNCaP cells treated with IFNα; however, this effect was reversed by STAT2 co-knockdown (Figure 4C; Supplementary Figure 10C). By performing RT-qPCR analysis, we confirmed that FOXA1 overexpression decreased the expression of a subset of STAT2 target genes in FOXA1-negative DU145 cells and that FOXA1 KD in FOXA1-high LNCaP cells increased expression of this subset of genes under IFNα stimulation (Figure 4, D and E). Similar to the impact on FOXA1 cistrome due to lower abundance of STAT2 compared to FOXA1 (Supplementary Figure 8), IFNα treatment or STAT2 KD had little or no effect on expression of FOXA1 target genes (both up- and down-regulated) in LNCaP cells (Supplementary Figure 11). These results indicate that FOXA1 inhibits expression of a set of IFNα-stimulated STAT2 target genes that are highly related to IFN signaling and immune response.

FOXA1 overexpression suppresses anti-cancer immune response in mice and patients. To determine whether FOXA1 inhibits anti-cancer immune response in vivo, we generated murine PCa TRAMP-C2 (lacking endogenous Foxa1 expression) stable cell lines expressing control vector, FOXA1-WT, DNA binding-deficient mutant FOXA1ΔαH3 or STAT2 binding deficient mutant FOXA1ΔSBR for animal studies. FOXA1 expression in these stable cell lines and their response to IFNα were confirmed by Western blot analysis (Supplementary Figure 12A) before they were injected s.c. into syngeneic C57BL/6 male mice. Poly(I:C) was intratumorally injected to trigger type I IFN immune response (39). Poly(I:C) administration decreased the growth of

control (TRAMP-C2-Vector) tumors in the majority of mice and prolonged the overall mouse survival (Figure 5, A and B; Supplementary Figure 12B). On the contrary, the growth-inhibitory effect of Poly(I:C) was largely diminished in tumors with overexpression of FOXA1-WT, FOXA1ΔαH3 but not FOXA1ΔSBR (Figure 5, A and B; Supplementary Figure 12B). Furthermore, TILs, especially $CD8^+$ T cells (including cytotoxic (Granzyme B^+) $CD8^+$ T cells), were discernibly increased in TRAMP-C2-Vector tumors treated with Poly(I:C); however, such effect was diminished in tumors with overexpression of FOXA1-WT, FOXA1ΔαH3 but not FOXA1ΔSBR (Supplementary Figure 12, C and D; Supplementary Figure 13A). The tumor response to Poly(I:C) treatment and FOXA1 expression was further reflected in expression of murine IFN signaling genes including *Isg15*, *Ifi44*, *H2-k1* and *Psmb9* (Supplementary Figure 13B). It is worth noting that FOXA1 and other FOXA subfamily members FOXA2 and FOXA3 share the similar forkhead (DNA binding) domains and the same SBR motifs in both human and mouse (Supplementary Figure 14A). Like FOXA1, both FOXA2 and FOXA3 also interacted with and suppressed IFN-induced transcriptional activity of STAT2 (Supplementary Figure 14, B and C). It has been reported that FOXA2 is expressed in neuroendocrine PCa (NEPC) (40). Compared to the typical NEPC cell line NCI-H660 and NE-like cell line PC-3, TRAMP-C2 cells express relatively low level of Foxa2 (Supplementary Figure 14D). The limited Foxa2 expression along with the observation that little or no Foxa1 is expressed in TRAMP-C2 cells is consistent with the finding that TRAMP-C2 tumors exhibited measurable anti-cancer immune response in mice. Consistent with these observations in the murine PCa model, meta-analysis of the data reported previously (41) showed that *Foxa1* mRNA level was much higher in resistant tumors compared to sensitive tumors while the IFN activity and expression of of T_{eff} cell markers such as *CD3e*, *CD8a* and *Gzmb* positively correlated with the response of murine breast tumors

to anti-PD1 and anti-CTLA-4 combined therapy (Figure 5C). These data support a role of Foxa1 in negatively regulating IFN signaling and immune response in prostate and breast cancer in mice.

Next, we examined whether FOXA1 overexpression confers resistance to ICI immunotherapy. We effectively knocked down endogenous Foxa1 in murine MyC-CaP PCa cell line using doxycycline-inducible shRNAs and demonstrated that Foxa1 knockdown enhanced IFN signaling in MyC-CaP cells following IFNα treatment (Figure 6A; Supplementary Figure 15A). We generated a syngeneic PCa mouse model using these stable MyC-CaP cell lines and treated mice with anti-PD1 and anti-CTLA-4 antibodies in combination with or without doxycycline. We demonstrated that knockdown of Foxa1 by doxycycline treatment enhanced the therapeutic efficacy of anti-PD1 and anti-CTLA-4 in MyC-CaP tumors (Figure 6B-E; Supplementary Figure 15, B and C). Knockdown of Foxa1 also increased IFN response gene expression and the accumulation of cytotoxic CD8 cells in MyC-CaP tumors (Figure 6, F and G; Supplementary Figure 15, B and C). These data not only indicate that FOXA1 mediates resistance to ICI immunotherapy, but also imply that FOXA1 is a viable target to sensitize PCa to ICIs.

To validate our findings from animal studies in clinical settings, we performed meta-analysis of the clinic data from castration-resistant prostate cancer (CRPC) patients treated by personalized peptide vaccines (PPV) (42). PPV is an immunotherapy that uses multiple cancer peptides knowingly associated with the preexisting host immunity. Previous phase III study suggestes that the median overall survival in PPV-treated patients with high lymphocytes was significantly longer than placebo-treated patients (43). By analyzing the gene expression and clinical data in the patients pretreated with PPV, we demonstrated that patients with high expression of *FOXA1* mRNA had lower overall survival (Supplementary Figure 15D). We

further showed that expression of IFN response and cytotoxic T cell marker genes such as *CD3E*, *PRF1* and *GZMB* were significantly lower in FOXA1-high tumors compared to FOXA1-low counterparts (Supplementary Figure 15D), supporting a possible IFN signal-inhibition and immune-suppression function of FOXA1 in PCa patients.

Activation of IFNs are required for anticancer immune responses elicited by chemotherapy and the IFN-related genetic signature correlates with clinical responses to this chemotherapeutic regimen in BCa (44). Immune response is also implicated in chemotherapy of BCa because higher levels of TILs prior to neo-adjuvant chemotherapy (NAC) are associated with higher rates of pathological complete response (pCR) (45, 46). To explore whether FOXA1 associates with the response of NAC-associated immune response, we analyzed RNA-seq data from the prospective BEAUTY study of BCa patients treated with NAC at Mayo Clinic (47) (Supplementary Figure 16A). We observed that *FOXA1* mRNA level was significantly higher in tumors without pCR (No-pCR) compared to tumors with pCR whereas the IFN activity was opposite (Figure 7A). In comparison with pCR tumors, non-pCR tumors expressed much lower levels of T_{eff} cell markers such as *CD3E*, *CD8A* and *GZMB* while having much higher expression of *FOXA1* (Figure 7A), supporting a role of FOXA1 in negatively regulating IFN signaling and immune response in BCa patients. The association of high FOXA1 expression with low IFN activity and NAC resistance was also observed in three independent BCa cohorts (Figure 7, B-D). Almost all luminal tumors in the Mayo Clinic cohort expressed FOXA1 at high levels, but had a very low rate of pCR (no single pCR case in luminal-A tumors and only 10.8% pCR rate in luminal-B tumors) (Supplementary Figure 16, A and B). FOXA1 is generally considered as a luminal gene. However, we did find that it was expressed in triple negative breast cancers (TNBC) although the expression level was lower compared to that in luminal subtypes

(Supplementary Figure 16B). While the overall pCR rate was very high (64%) in TNBC (Supplementary Figure 16A), there was no statistically significant difference in FOXA1 expression between pCR and non-pCR in the TNBC cohort (Supplementary Figure 16B). One possible reason could be the small sample size of TNBC cases (n = 42) in the Mayo Clinic cohort. This notion is supported by the finding from a larger cohort (n = 119) of NAC-treated TNBC where *FOXA1* mRNA level was significantly higher in non-pCR TNBC than those with pCR (Supplementary Figure 16C). Intriguingly, neither NAC responsiveness nor FOXA1 expression was associated with TMB in the Mayo Clinic cohort (Supplementary Figure 16, D and E). These results suggest that FOXA1 overepression confers resistance to NAC.

In addition to prostate adenocarcinoma and luminal breast cancer, two steroid hormone-driven cancers, bladder cancer is the third cancer type in the TCGA database that has the highest expression of *FOXA1* (Figure 8A). Therefore, we were also interested in evaluating the association of FOXA1 with IFN activation and ICI immunotherapy response in bladder cancer, a malignancy not necessarily driven by AR or ER. Similar to the results in prostate and breast cancer, *FOXA1* expression inversely correlated with the levels of IFN response signature and APM genes, but not TMB (Figure 8, B and C). FOXA1 can also bind to STAT proteins and suppress IFN signaling in bladder cancer cells (Supplementary Figure 17). Furthermore, we examined FOXA1 protein expression using immunohistochemistry (IHC) in a set of twenty-two urothelial carcinomas of the bladder, ureter and renal pelvis collected prior to anti-PD1 therapy. We found that patients with tumors expressing higher FOXA1 protein levels had much lower rates of progression-free survival (Figure 8D; Supplementary Figure 18; Supplementary Table 3). Similar results were also obtained from bladder cancer patients treated with Bacillus Calmette-Guerin (BCG) immunotherapy (48) (Supplementary Figure 19A) or chemotherapy of

methotrexate, vinblastine, doxorubicin, and cisplatin (MVAC) (49) (Supplementary Figure 19B). Together, the data from prostate, breast and bladder cancer patients suggest that FOXA1 overexpression contributes to immune evasion and immuno- and chemotherapy resistance in clinic.

Discussion

Genetic inactivation (deletions or inactivation mutations) of genes encoding IFN response/receptor and antigen presentation pathway proteins has been linked to immune evasion of human cancers such as melanoma (7, 18, 22, 23). In the present study we demonstrate that FOXA1 directly binds a large portion (more than two-thirds) of the STAT2 DNA binding domain and inhibits STAT2 binding of its DNA binding sequence (ISRE). Through genome-wide ChIP-seq and RNA-seq analysis, we further show that overexpressed FOXA1 prohibits STAT2 occupancy on gene loci harboring a typical STAT2 DNA binding motif and impedes expression of STAT2 targets including IFN signaling and APM genes. We also provide evidence that FOXA1 overexpression not only inhibits anti-cancer immune response in mice, but also associates with decreased expression of IFN response and cytotoxic T cell marker genes in patient samples. Our findings therefore reveal FOXA1 overexpression-mediated inhibition of STAT2 DNA binding activity and transcriptional suppression of IFN signaling and antigen presentation gene expression as a new mechanism of cancer cell escaping from immune surveillance (Figure 9).

TMB has been linked to neoantigen availability and immune response to ICIs in various human cancers, especially those cancer types with high TMB such as melanoma and non-small cell lung cancer (50-52). It has been affirmed by multiple studies that PCa possesses a lower

TMB rate than many other epithelial tumor types (27, 50, 53). Low TMB appears to be a possible reason for the "coldness" of PCa to immunotherapy. However, response to ICIs is not significantly associated with TMB in some cancers such as breast cancer (4). Increasing evidence indicates that high IFNγ response gene expression is necessarily required for response to ICIs in PCa with low TMB (6). Of note, a recent clinical study shows that responders do not have significantly higher TMB than nonresponders when stratified by melanoma subtypes (5). In our study, we found that there was little or no association of TMB with FOXA1 expression, infiltration of $CD8^+$ T_{eff} cells or NAC chemotherapy efficacy in different BCa cohorts. These observations suggest that TMB is not the only major player affecting the therapeutic efficiency of ICIs, but other factors such as IFN activation in cancer are also critical for ICI response. This notion is further supported by our finding that FOXA1 overexpression causes IFN suppression, immune evasion and immunotherapy resistance in cancer. However, a limitation in our study in bladder cancer is that we do not have the high throughput sequencing data of TMB in tumor samples treated with anti-PD1 immunotherapy and therefore future investigation is warranted to determine whether or not FOXA1 overeperssion correlates with anti-PD resistance in blader cancer patients with high TMB.

FOXA1 is a well-known pioneer factor due to its function in activation of steroid hormone receptors such as AR and ER, and its expression is essential for maintenance of the luminal phenotype of PCa and BCa (24-26). AR^+ PCa and ER^+ BCa are generally less responsive to immunotherapies (3, 54, 55). It is highly relevant to explore whether the immune irresponsiveness in these two cancer types is related to luminal epithelial origins, hormone-dependence or other factors commonly present in PCa and BCa such as the pioneer factor FOXA1. We demonstrated that FOXA1 expression inversely correlates with expression of IFN

response and APM genes in both PCa and BCa; however, the association is unrelated to tumor stages such as primary PCa versus CRPC, suggesting that the correlation appears not entirely hormone-related. High level of TILs has been shown to be associated with favorable response to NAC in BCa (45, 56). Similar to the response to immunotherapy in PCa, we found that high level of FOXA1 also associates with reduced IFN activity and T cell infiltration in BCa treated with NAC. While BCa can be divided into multiple molecular subtypes with distinct traits such as luminal versus TNBC, similar to the outcome in luminal BCa, a significant association of high-level FOXA1 expression with NAC response was also detected in TNBC even when the luminal AR^+ (LAR) TNBC was excluded. Thus, our data pinpoint that FOXA1 overexpression rather than luminal epithelial origins or hormone-dependence is one of the key factors contributing to the immunotherapy irresponsiveness in both PCa and BCa.

The importance of the pioneer factor function of FOXA1 in PCa and BCa is further accentuated by the finding that the *FOXA1* gene is frequent mutations in human cancers such as PCa and BCa (27-30). FOXA1 mutants are reported to drive proliferation of cancer cells or organoids cultured in vitro and tumor growth in immune-deficient mice in a manner dependent on its pioneer factor activities such as DNA binding and chromatin regulation (29, 30). However, the role of FOXA1 mutations in regulation of cancer immune response has not been explored. Our findings from cancer cell lines, mouse tumors and patient samples indicate that FOXA1 inhibition of IFN and APM signaling is independent of the missense and C-terminal truncation mutations of FOXA1 detected in human cancers. Moreover, we provide evidence that FOXA1 suppresses IFN signaling gene expression and cancer immune response and that this effect does not dependent on its DNA binding function. Our results indicate that besides via its gene mutation-mediated cell proliferation and invasion, FOXA1 can also drive cancer progression

through overexpression-mediated suppression of IFN signaling and inhibition of cancer immune response in a manner independent of its pioneer factor function (Figure 9).

In summary, we identify FOXA1 overexpression-mediated suppression of STAT2 DNA binding and IFN signaling gene expression as a new mechanism of immune evasion in different cancer types including prostate, breast and bladder cancers. This newly discovered role of FOXA1 is neither dependent on its pioneer factor function nor its mutations detected in human cancers. Our findings stress that prospective studies are warranted to investigate whether FOXA1 overexpression could be a potential prognostic factor to predict immunotherapy response in a manner independent of luminal cell origins or TMB of tumors. Our results also imply that further exploration is needed to determine whether eliminating FOXA1 protein could be a viable strategy to turn FOXA1-overexpressed "immune-cold" tumors into "immune-hot" tumors. Pioneer factors such as FOXA1 are notoriously difficult to target and currently there are no clinical-grade agents that target FOXA1. The emerging technology Proteolysis Targeting Chimeras (PROTACs), especially the olionucleotide-based PROTACs (57) could be a promising option to develop novel anti-cancer agents to target FOXA1.

Methods

Single cell RNA sequencing data analysis. Detailed clinic information of prostate cancer samples used for single cell RNA-seq is provided in Supplementary Table 1. For data generated with 10X platform, raw data was processed using Cell Ranger (v2.1.0) into UMI matrix. The maximum number of cells in one sample was estimated by cell ranger across 13 samples and was used as the estimation of cell number. For each cell, we calculated three quality measures: percent of mitochondrial genes, number of total genes and housekeeping genes expressed (58). We

removed cells that have higher than 20% expression on mitochondrial genes, lower than 200 or higher than 5218 total genes expressed, or lower than 56 housekeeping genes expressed (58). The resultant gene expression matrix was imported into R (v3.5.1) statistical environment for further analysis. Data normalization and annotation was performed using R package scran (v1.10.2). To calculate pool-based normalization factor, cells for each sample were first splited into sensible clusters using quickCluster function (max.size = 3000). The fastMNN function (k = 5, d = 50, approximate = TRUE, auto.order = TRUE) was used to apply mutual nearest neighbor method to correct for batch effect among samples. Similarly, the single cell RNA-seq from breast cancer (GSE140819 including: GSM4186971, GSM4186973, GSM4186975, GSM4186977, GSM4186972, GSM4186980) (35) was analyzed accordingly. To investigate the expression correlation between *FOXA1* level and the expression of IFN response signature genes as well as antigen presentation machinery (APM) genes, these genes were ranked according to the increased levels of *FOXA1* transcript revealed by the single cell RNA-seq data from prostate or breast cancers as descripted above and heatmaps were generated accordingly.

IFN activity score and gene expression correlation analysis. To calculate the IFN activity score and other gene expression activity scores, gene expression values Log2(FPKM+1) of each sample were converted to Z-scores by $Z = (x - \mu)/\sigma$, where μ is the average gene expression values across all samples of a gene and σ is the standard deviation of the gene expression values across all samples of a gene. The Z-scores were then summed across all genes for each sample to represent the gene expression activity score. The summed Z-scores were converted to a percentile and normalized between 0 and 1 with 0 being the lowest and 1 being the highest in Figure S1D and S1E. The IFN response signature or activity genes (*ACACB, BIRC3, BST2,*

CXCL1,CXCL2, DDX60, DHX58,GBP1, HERC5, IFI16, IFI27, IFI44, IFI44L, IFIH1, IFIT3, IFITM1, IRF7, ISG15, ISG20 ,LGALS9, MX1 ,OAS1, OAS2, PARP12, RASGRP3 , SAMD9 , SERPING1 , SLC15A3, SP110, STAT1 ,XAF1) which has been shown to be associated with favorable prognosis in melanoma (39) and antigen presentation machinery (APM) genes (*B2M, HLA-A, HLA-B HLA-C, HLA-E, HLA-F, HLA-G, HLA-H, HLA-J, PSMB8, PSMB9, TAP1, TAP2, TAPBP*) were included in the analyses as many as possible unless the expression data of specific gene(s) is not available in the dataset.

To identify which factors contribute to the suppression of IFN activity in immunologically "cold" tumors, we analyzed RNA-seq expression data from TCGA cohorts of prostate cancer (n = 490) (53) and breast cancer (n = 960) (59) and generated a list of genes whose expression negatively correlated with IFN activity by performing Spearman's rho rank analysis. Genes commonly present in the list of the top hits in both prostate and breast cancer cohorts were considered further as the potential candidate(s) that may be able to suppress IFN activity in immunologically "cold" cancers such as prostate and breast cancer. All data was derived from cBioPortal (http://www.cbioportal.org/) (60).

To investigate the expression correlation between *FOXA1* level and IFN response signature genes or antigen presentation machinery (APM) genes, these genes were ranked according to the increased levels of *FOXA1* transcript revealed by bulk tissue RNA-seq data from prostate cancer (TCGA, n = 490) (53), metastatic prostate cancer (SU2C/PCF Dream Team, source of file: data_mRNA_seq_fpkm_polya.txt, n = 270) (61), bone metastatic prostate cancer from Mayo Clinic (dbGaP: phs001141.v1.p1, n = 54) (62), breast cancer from TCGA (n = 960) (59), breast cancer from METABRIC database (n = 1904) (63) and bladder cancer from TCGA (n = 404) (64) and heatmaps were generated accordingly. The expression levels of IFN response signature

genes and APM genes were scored. Their correlations with *FOXA1* expression were determined based on the Pearson's r-values and *P*-values.

Chromatin immunoprecipitation sequencing (ChIP-seq) and bioinformatics analyses. For ChIP experiments, cells were cross-linked for 15 min at room temperature with 1% formaldehyde/PBS solution. Cross-linked chromatin was sonicated, diluted and immunoprecipitated with Protein A/G agarose prebound with antibodies at 4°C overnight. Antibodies for ChIP were STAT2 (2 μg/sample; #72604S, Cell Signaling Technology), FOXA1 (2 μg/sample; #ab23738, Abcam). Precipitated protein-DNA complexes were eluted and cross-linking was reversed at 65°C for 12 h. High-throughput sequencing (51 nt, pair-end) was performed using the Illumina HiSeq™ 4000 platforms at the Mayo Genome Core Facility. All short reads were mapped to the human reference genome (GRCh38/hg38) using bowtie2 (version 2.1.0) with default configurations. Reads mapped to multiple positions (greater than 2) were discarded, and the remained reads were used for peak calling using MACS2 (version 2.0.10) with a *P* value cutoff of 1e-5 (macs2 call peak -bdg -SPTMR -f BAM -p 1e-5) (65). Peaks located in the blacklists such as centromere regions were removed (https://sites.google.com/site/anshulkundaje/projects/blacklists). ChIP-seq tag intensity tracks (bedGraph files) were generated by MACS2, and converted into bigWig files using UCSC "wigToBigWig" tool. Heat maps were drawn by deepTools 2.0. A set of peaks identified by ChIP-seq were validated by qPCR using Power SYBR Green (Thermo Fisher Scientific, # 4368708). Primer sequences used for ChIP-qPCR are listed in Supplementary Table 4.

Statistical analysis. GraphPad Prism version 8.0 or SPSS version 17.0 were used for statistical analyses of results from RT-qPCR, luciferase reporter and cell proliferation assays. Other statistical analyses were conducted in the statistical computing environment R (v. 3.3.1). Statistical comparison was done using Mann-Whitney U test or one-way analysis of variance (ANOVA) with Bonferroni correction for multiple tests. Since treatment and time course was investigated, two-way analysis of variance (ANOVA) was also applied. Spearman's rho correlation test and Pearson correlation test were used for testing statistical significance of correlation. Statistical analysis is specifically described in figure legends. P value < 0.05 was considered significant.

Study approval. The protocol for the animal experiments including TRAMP-C2 murine PCa model and MyC-CaP murine PCa model were approved by the Mayo Clinic Institutional Animal Cure and Use Committee (IACUC). The protocol for study of urothelial carcinoma treated with anti-PD1 immunotherapy was approved by the Ethical and Scientific Committee (equivalent to Institutional Review Board (IRB)) at Fudan University Shanghai Cancer Center. All patients provided written consent before enrolling in the study.

Acknowledgments

This work was supported in part by the National Institutes of Health R01 CA130908 and CA203849 (to H.H.); the Mayo Clinic Foundation (to H.H.); Mayo Clinic Breast SPORE P50CA116201-9 (to M.P.G., L.W., K.R. K., V. S.); Mayo Clinic Cancer Center Support Grant P50CA015083; Mayo Clinic Center for Individualized Medicine; Nadia's Gift Foundation; John P. Guider; The Eveleigh Family; George M. Eisenberg Foundation for Charities; Prospect Creek

Foundation; Randy Shaver Cancer Research and Community Fund. Y.H. is supported by Mayo Clinic Edward C. Kendall Fellowship.

Author contributions

Conception and design, H.H. and Y.H.; Acquisition of data, Y.H., S.R., M.P.G, D.P.H., and S.H.; Analysis and interpretation of data, Y.H., L.(Liguo) W., T.W., Y.X., D.P.H., K.R.K., Z.Y., H.S. and X.T.; Preparation of the manuscript, H.H., S.R., Y.H., M.P.G., C.M.P., H.D., V.S.S, L.(Liguo) W., T.W. and Y.Y.; Administrative, technical, or material support, J.M.C., D.Y., H.D., J.M., S.W., H.X., Y.P., L. (Liewei) W., R.W., J.C.B., S.J.W., X.H., X.Z., A.H.B. and C.M.P.; Supervision, H.H. and S.R.

Conflict of interest: The authors declare no conflict of interest.

References

1. Wei SC, Duffy CR, and Allison JP. Fundamental Mechanisms of Immune Checkpoint Blockade Therapy. *Cancer Discov.* 2018;8(9):1069-86.
2. Rescigno P, and de Bono JS. Immunotherapy for lethal prostate cancer. *Nat Rev Urol.* 2019;16(2):69-70.
3. Esteva FJ, Hubbard-Lucey VM, Tang J, and Pusztai L. Immunotherapy and targeted therapy combinations in metastatic breast cancer. *Lancet Oncol.* 2019;20(3):e175-e86.
4. Samstein RM, Lee CH, Shoushtari AN, Hellmann MD, Shen R, Janjigian YY, et al. Tumor mutational load predicts survival after immunotherapy across multiple cancer types. *Nat Genet.* 2019;51(2):202-6.
5. Liu D, Schilling B, Liu D, Sucker A, Livingstone E, Jerby-Arnon L, et al. Integrative molecular and clinical modeling of clinical outcomes to PD1 blockade in patients with metastatic melanoma. *Nat Med.* 2019;25(12):1916-27.
6. Subudhi SK, Vence L, Zhao H, Blando J, Yadav SS, Xiong Q, et al. Neoantigen responses, immune correlates, and favorable outcomes after ipilimumab treatment of patients with prostate cancer. *Sci Transl Med.* 2020;12(537).
7. Gao J, Shi LZ, Zhao H, Chen J, Xiong L, He Q, et al. Loss of IFN-gamma Pathway Genes in Tumor Cells as a Mechanism of Resistance to Anti-CTLA-4 Therapy. *Cell.* 2016;167(2):397-404 e9.
8. Ishizuka JJ, Manguso RT, Cheruiyot CK, Bi K, Panda A, Iracheta-Vellve A, et al. Loss of ADAR1 in tumours overcomes resistance to immune checkpoint blockade. *Nature.* 2019;565(7737):43-8.
9. Kranz LM, Diken M, Haas H, Kreiter S, Loquai C, Reuter KC, et al. Systemic RNA delivery to dendritic cells exploits antiviral defence for cancer immunotherapy. *Nature.* 2016;534(7607):396-401.
10. Borden EC. Interferons alpha and beta in cancer: therapeutic opportunities from new insights. *Nat Rev Drug Discov.* 2019;18(3):219-34.
11. Aznar MA, Planelles L, Perez-Olivares M, Molina C, Garasa S, Etxeberria I, et al. Immunotherapeutic effects of intratumoral nanoplexed poly I:C. *J Immunother Cancer.* 2019;7(1):116.
12. Chiappinelli KB, Strissel PL, Desrichard A, Li H, Henke C, Akman B, et al. Inhibiting DNA Methylation Causes an Interferon Response in Cancer via dsRNA Including Endogenous Retroviruses. *Cell.* 2015;162(5):974-86.
13. Ayers M, Lunceford J, Nebozhyn M, Murphy E, Loboda A, Kaufman DR, et al. IFN-gamma-related mRNA profile predicts clinical response to PD-1 blockade. *J Clin Invest.* 2017;127(8):2930-40.
14. Borden EC, Sen GC, Uze G, Silverman RH, Ransohoff RM, Foster GR, et al. Interferons at age 50: past, current and future impact on biomedicine. *Nat Rev Drug Discov.* 2007;6(12):975-90.
15. Rizvi NA, Hellmann MD, Snyder A, Kvistborg P, Makarov V, Havel JJ, et al. Cancer immunology. Mutational landscape determines sensitivity to PD-1 blockade in non-small cell lung cancer. *Science.* 2015;348(6230):124-8.
16. Rooney MS, Shukla SA, Wu CJ, Getz G, and Hacohen N. Molecular and genetic properties of tumors associated with local immune cytolytic activity. *Cell.* 2015;160(1-2):48-61.
17. Van Allen EM, Miao D, Schilling B, Shukla SA, Blank C, Zimmer L, et al. Genomic correlates of response to CTLA-4 blockade in metastatic melanoma. *Science.* 2015;350(6257):207-11.
18. Restifo NP, Marincola FM, Kawakami Y, Taubenberger J, Yannelli JR, and Rosenberg SA. Loss of functional beta 2-microglobulin in metastatic melanomas from five patients receiving immunotherapy. *J Natl Cancer Inst.* 1996;88(2):100-8.

19. Leach DR, Krummel MF, and Allison JP. Enhancement of antitumor immunity by CTLA-4 blockade. *Science.* 1996;271(5256):1734-6.
20. Le DT, Uram JN, Wang H, Bartlett BR, Kemberling H, Eyring AD, et al. PD-1 Blockade in Tumors with Mismatch-Repair Deficiency. *N Engl J Med.* 2015;372(26):2509-20.
21. Sharma P, and Allison JP. The future of immune checkpoint therapy. *Science.* 2015;348(6230):56-61.
22. Zaretsky JM, Garcia-Diaz A, Shin DS, Escuin-Ordinas H, Hugo W, Hu-Lieskovan S, et al. Mutations Associated with Acquired Resistance to PD-1 Blockade in Melanoma. *N Engl J Med.* 2016;375(9):819-29.
23. Davoli T, Uno H, Wooten EC, and Elledge SJ. Tumor aneuploidy correlates with markers of immune evasion and with reduced response to immunotherapy. *Science.* 2017;355(6322).
24. Lupien M, Eeckhoute J, Meyer CA, Wang Q, Zhang Y, Li W, et al. FoxA1 translates epigenetic signatures into enhancer-driven lineage-specific transcription. *Cell.* 2008;132(6):958-70.
25. Carroll JS, Liu XS, Brodsky AS, Li W, Meyer CA, Szary AJ, et al. Chromosome-wide mapping of estrogen receptor binding reveals long-range regulation requiring the forkhead protein FoxA1. *Cell.* 2005;122(1):33-43.
26. Jozwik KM, and Carroll JS. Pioneer factors in hormone-dependent cancers. *Nat Rev Cancer.* 2012;12(6):381-5.
27. Barbieri CE, Baca SC, Lawrence MS, Demichelis F, Blattner M, Theurillat JP, et al. Exome sequencing identifies recurrent SPOP, FOXA1 and MED12 mutations in prostate cancer. *Nat Genet.* 2012;44(6):685-9.
28. Grasso CS, Wu YM, Robinson DR, Cao X, Dhanasekaran SM, Khan AP, et al. The mutational landscape of lethal castration-resistant prostate cancer. *Nature.* 2012;487(7406):239-43.
29. Adams EJ, Karthaus WR, Hoover E, Liu D, Gruet A, Zhang Z, et al. FOXA1 mutations alter pioneering activity, differentiation and prostate cancer phenotypes. *Nature.* 2019;571(7765):408-12.
30. Parolia A, Cieslik M, Chu SC, Xiao L, Ouchi T, Zhang Y, et al. Distinct structural classes of activating FOXA1 alterations in advanced prostate cancer. *Nature.* 2019;571(7765):413-8.
31. Arruabarrena-Aristorena A, Maag JLV, Kittane S, Cai Y, Karthaus WR, Ladewig E, et al. FOXA1 Mutations Reveal Distinct Chromatin Profiles and Influence Therapeutic Response in Breast Cancer. *Cancer Cell.* 2020.
32. Eggermont AMM, Blank CU, Mandala M, Long GV, Atkinson V, Dalle S, et al. Adjuvant Pembrolizumab versus Placebo in Resected Stage III Melanoma. *N Engl J Med.* 2018;378(19):1789-801.
33. Gandhi L, Rodriguez-Abreu D, Gadgeel S, Esteban E, Felip E, De Angelis F, et al. Pembrolizumab plus Chemotherapy in Metastatic Non-Small-Cell Lung Cancer. *N Engl J Med.* 2018;378(22):2078-92.
34. Rini BI, Plimack ER, Stus V, Gafanov R, Hawkins R, Nosov D, et al. Pembrolizumab plus Axitinib versus Sunitinib for Advanced Renal-Cell Carcinoma. *N Engl J Med.* 2019;380(12):1116-27.
35. Slyper M, Porter CBM, Ashenberg O, Waldman J, Drokhlyansky E, Wakiro I, et al. A single-cell and single-nucleus RNA-Seq toolbox for fresh and frozen human tumors. *Nat Med.* 2020;26(5):792-802.
36. Chung W, Eum HH, Lee HO, Lee KM, Lee HB, Kim KT, et al. Single-cell RNA-seq enables comprehensive tumour and immune cell profiling in primary breast cancer. *Nat Commun.* 2017;8:15081.
37. Clark KL, Halay ED, Lai E, and Burley SK. Co-crystal structure of the HNF-3/fork head DNA-recognition motif resembles histone H5. *Nature.* 1993;364(6436):412-20.

38. Pomerantz MM, Qiu X, Zhu Y, Takeda DY, Pan W, Baca SC, et al. Prostate cancer reactivates developmental epigenomic programs during metastatic progression. *Nat Genet.* 2020;52(8):790-9.
39. Bald T, Landsberg J, Lopez-Ramos D, Renn M, Glodde N, Jansen P, et al. Immune cell-poor melanomas benefit from PD-1 blockade after targeted type I IFN activation. *Cancer Discov.* 2014;4(6):674-87.
40. Park JW, Lee JK, Witte ON, and Huang J. FOXA2 is a sensitive and specific marker for small cell neuroendocrine carcinoma of the prostate. *Mod Pathol.* 2017;30(9):1262-72.
41. Hollern DP, Xu N, Thennavan A, Glodowski C, Garcia-Recio S, Mott KR, et al. B Cells and T Follicular Helper Cells Mediate Response to Checkpoint Inhibitors in High Mutation Burden Mouse Models of Breast Cancer. *Cell.* 2019;179(5):1191-206 e21.
42. Araki H, Pang X, Komatsu N, Soejima M, Miyata N, Takaki M, et al. Haptoglobin promoter polymorphism rs5472 as a prognostic biomarker for peptide vaccine efficacy in castration-resistant prostate cancer patients. *Cancer Immunol Immunother.* 2015;64(12):1565-73.
43. Noguchi M, Fujimoto K, Arai G, Uemura H, Hashine K, Matsumoto H, et al. A randomized phase III trial of personalized peptide vaccination for castrationresistant prostate cancer progressing after docetaxel. *Oncol Rep.* 2021;45(1):159-68.
44. Sistigu A, Yamazaki T, Vacchelli E, Chaba K, Enot DP, Adam J, et al. Cancer cell-autonomous contribution of type I interferon signaling to the efficacy of chemotherapy. *Nat Med.* 2014;20(11):1301-9.
45. Denkert C, von Minckwitz G, Brase JC, Sinn BV, Gade S, Kronenwett R, et al. Tumor-infiltrating lymphocytes and response to neoadjuvant chemotherapy with or without carboplatin in human epidermal growth factor receptor 2-positive and triple-negative primary breast cancers. *J Clin Oncol.* 2015;33(9):983-91.
46. Savas P, Salgado R, Denkert C, Sotiriou C, Darcy PK, Smyth MJ, et al. Clinical relevance of host immunity in breast cancer: from TILs to the clinic. *Nat Rev Clin Oncol.* 2016;13(4):228-41.
47. Goetz MP, Kalari KR, Suman VJ, Moyer AM, Yu J, Visscher DW, et al. Tumor Sequencing and Patient-Derived Xenografts in the Neoadjuvant Treatment of Breast Cancer. *J Natl Cancer Inst.* 2017;109(7).
48. Kim YJ, Ha YS, Kim SK, Yoon HY, Lym MS, Kim MJ, et al. Gene signatures for the prediction of response to Bacillus Calmette-Guerin immunotherapy in primary pT1 bladder cancers. *Clin Cancer Res.* 2010;16(7):2131-7.
49. McConkey DJ, Choi W, Shen Y, Lee IL, Porten S, Matin SF, et al. A Prognostic Gene Expression Signature in the Molecular Classification of Chemotherapy-naive Urothelial Cancer is Predictive of Clinical Outcomes from Neoadjuvant Chemotherapy: A Phase 2 Trial of Dose-dense Methotrexate, Vinblastine, Doxorubicin, and Cisplatin with Bevacizumab in Urothelial Cancer. *Eur Urol.* 2016;69(5):855-62.
50. Alexandrov LB, Nik-Zainal S, Wedge DC, Aparicio SA, Behjati S, Biankin AV, et al. Signatures of mutational processes in human cancer. *Nature.* 2013;500(7463):415-21.
51. Snyder A, Makarov V, Merghoub T, Yuan J, Zaretsky JM, Desrichard A, et al. Genetic basis for clinical response to CTLA-4 blockade in melanoma. *N Engl J Med.* 2014;371(23):2189-99.
52. Hellmann MD, Nathanson T, Rizvi H, Creelan BC, Sanchez-Vega F, Ahuja A, et al. Genomic Features of Response to Combination Immunotherapy in Patients with Advanced Non-Small-Cell Lung Cancer. *Cancer Cell.* 2018;33(5):843-52 e4.
53. Cancer Genome Atlas Research N. The Molecular Taxonomy of Primary Prostate Cancer. *Cell.* 2015;163(4):1011-25.
54. Venturini NJ, and Drake CG. Immunotherapy for Prostate Cancer. *Cold Spring Harb Perspect Med.* 2019;9(5).

55. Rescigno P, and de Bono JS. Immunotherapy for lethal prostate cancer. *Nat Rev Urol.* 2019;16(2):69-70.
56. Salgado R, Denkert C, Campbell C, Savas P, Nuciforo P, Aura C, et al. Tumor-Infiltrating Lymphocytes and Associations With Pathological Complete Response and Event-Free Survival in HER2-Positive Early-Stage Breast Cancer Treated With Lapatinib and Trastuzumab: A Secondary Analysis of the NeoALTTO Trial. *JAMA Oncol.* 2015;1(4):448-54.
57. Paiva SL, and Crews CM. Targeted protein degradation: elements of PROTAC design. *Curr Opin Chem Biol.* 2019;50:111-9.
58. Tirosh I, Izar B, Prakadan SM, Wadsworth MH, 2nd, Treacy D, Trombetta JJ, et al. Dissecting the multicellular ecosystem of metastatic melanoma by single-cell RNA-seq. *Science.* 2016;352(6282):189-96.
59. Cancer Genome Atlas N. Comprehensive molecular portraits of human breast tumours. *Nature.* 2012;490(7418):61-70.
60. Cerami E, Gao J, Dogrusoz U, Gross BE, Sumer SO, Aksoy BA, et al. The cBio cancer genomics portal: an open platform for exploring multidimensional cancer genomics data. *Cancer Discov.* 2012;2(5):401-4.
61. Abida W, Cyrta J, Heller G, Prandi D, Armenia J, Coleman I, et al. Genomic correlates of clinical outcome in advanced prostate cancer. *Proc Natl Acad Sci U S A.* 2019;116(23):11428-36.
62. Wang L, Dehm SM, Hillman DW, Sicotte H, Tan W, Gormley M, et al. A prospective genome-wide study of prostate cancer metastases reveals association of wnt pathway activation and increased cell cycle proliferation with primary resistance to abiraterone acetate-prednisone. *Ann Oncol.* 2018;29(2):352-60.
63. Pereira B, Chin SF, Rueda OM, Vollan HK, Provenzano E, Bardwell HA, et al. The somatic mutation profiles of 2,433 breast cancers refines their genomic and transcriptomic landscapes. *Nat Commun.* 2016;7:11479.
64. Robertson AG, Kim J, Al-Ahmadie H, Bellmunt J, Guo G, Cherniack AD, et al. Comprehensive Molecular Characterization of Muscle-Invasive Bladder Cancer. *Cell.* 2017;171(3):540-56 e25.
65. Zhang Y, Liu T, Meyer CA, Eeckhoute J, Johnson DS, Bernstein BE, et al. Model-based analysis of ChIP-Seq (MACS). *Genome Biol.* 2008;9(9):R137.

Figure 1

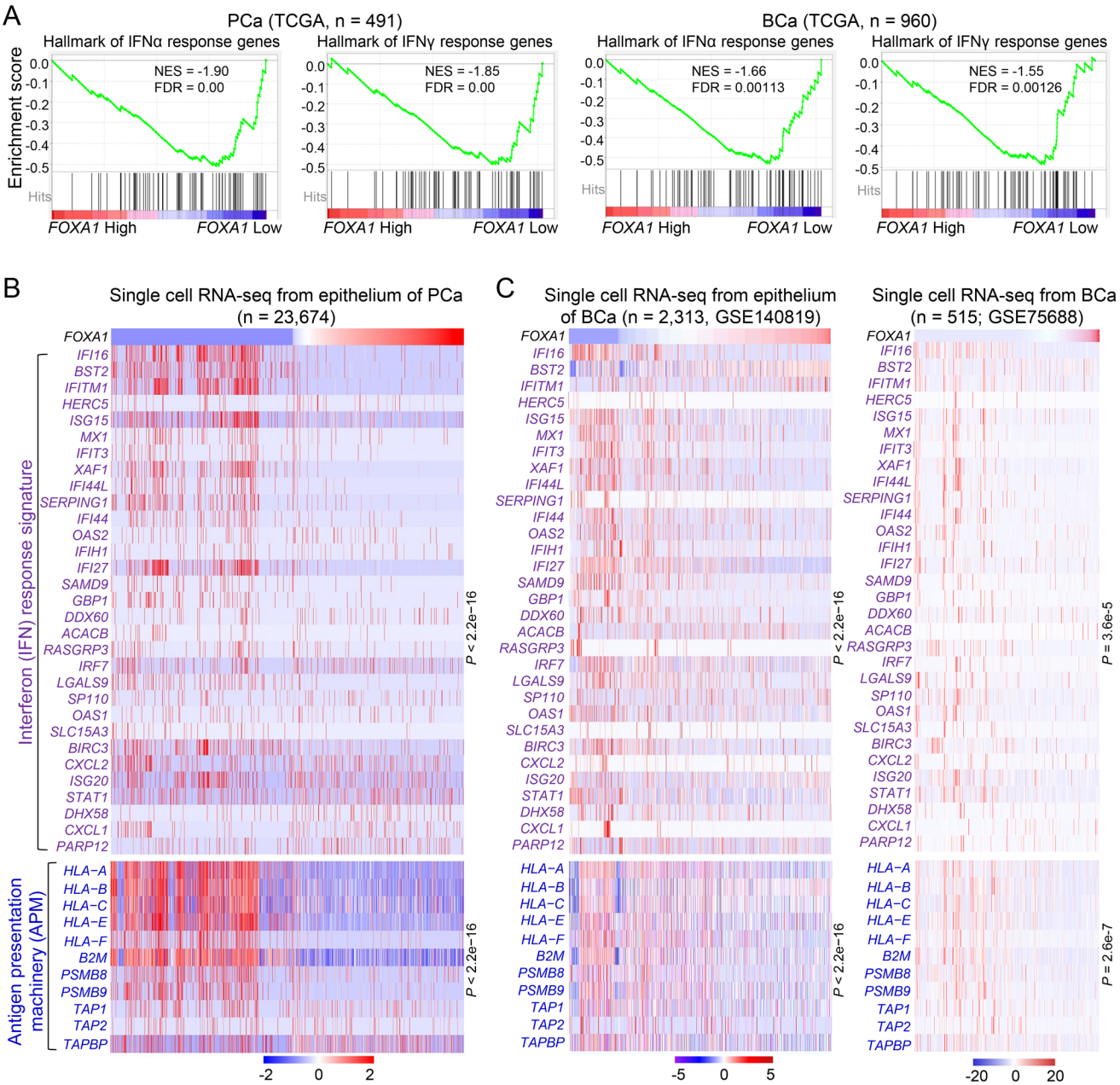

Figure 1. *FOXA1* levels inversely correlate with interferon signaling gene expression in prostate and breast cancer. (**A**) GSEA enrichment plots show the inverse correlation between *FOXA1* expression and IFN response hallmark genes in PCa and BCa from TCGA database. The *FOXA1* high and low groups were defined using the median as the cutoff. (**B** and **C**) Heatmaps show the inverse correlation of *FOXA1* expression with IFN response signature genes and APM genes in single cell RNA-seq data of PCa (**B**) and BCa (**C**) samples. Statistical significance was determined by Pearson correlation test.

Figure 2

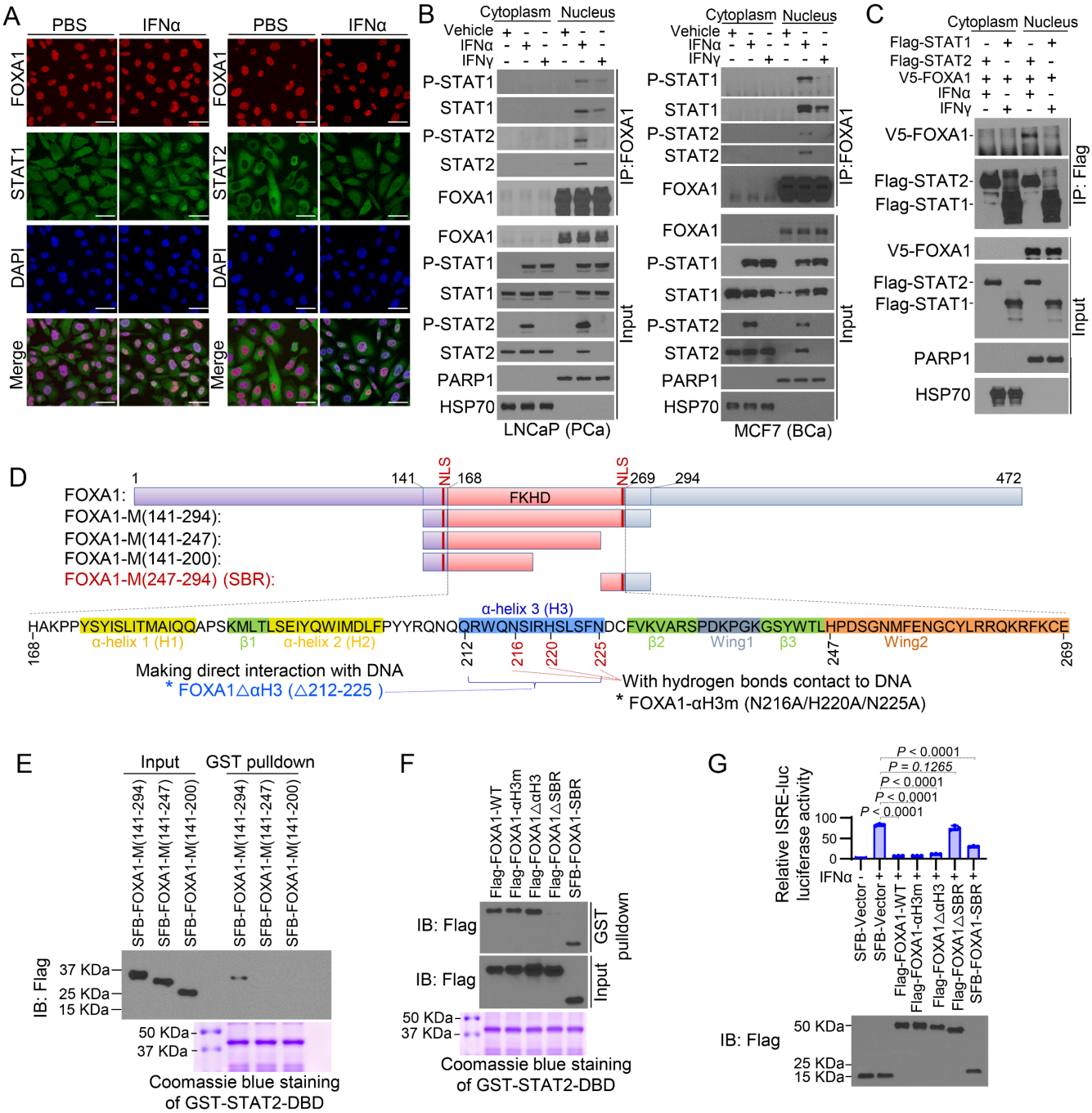

Figure 2. FOXA1 binds STAT2 DBD and impedes STAT2 DNA binding ability. (**A**) Immunofluorescence chemistry analysis of STAT1, STAT2 and FOXA1 in LNCaP cells treated with vehicle (PBS) or IFNα. (**B**) Co-IP shows the interaction of FOXA1 with STAT1 and STAT2 at the endogenous level in LNCaP and MCF7 cells treated with IFNα or IFNγ. (**C**) Co-IP analysis of interaction among ectopically expressed FOXA1, STAT1, and STAT2 proteins in 293T cells. (**D**) Diagram shows the domain structure of FOXA1 forkhead (FKHD) DNA binding domain and FOXA1 truncation and missense mutation expression constructs. NLS, nuclear localization signal; SBR, STAT2 binding region. (**E** and **F**) GST pulldown assay shows the interaction of GST-tagged STAT2 DBD with the indicated FOXA1 mutants expressed in 293T cells. WT, wild type; ΔαH3, deletion of α-helix 3; ΔSBR, deletion of STAT2 binding region. (**G**) Luciferase reporter assay shows the inhibitory effect of the indicated FOXA1 WT or mutants on ISRE-luc reporter gene activity in DU145 cells. Data shown as means ± SD (n = 3). Statistical significance was determined by one-way ANOVA with Bonferroni correction for multiple tests.

Figure 3

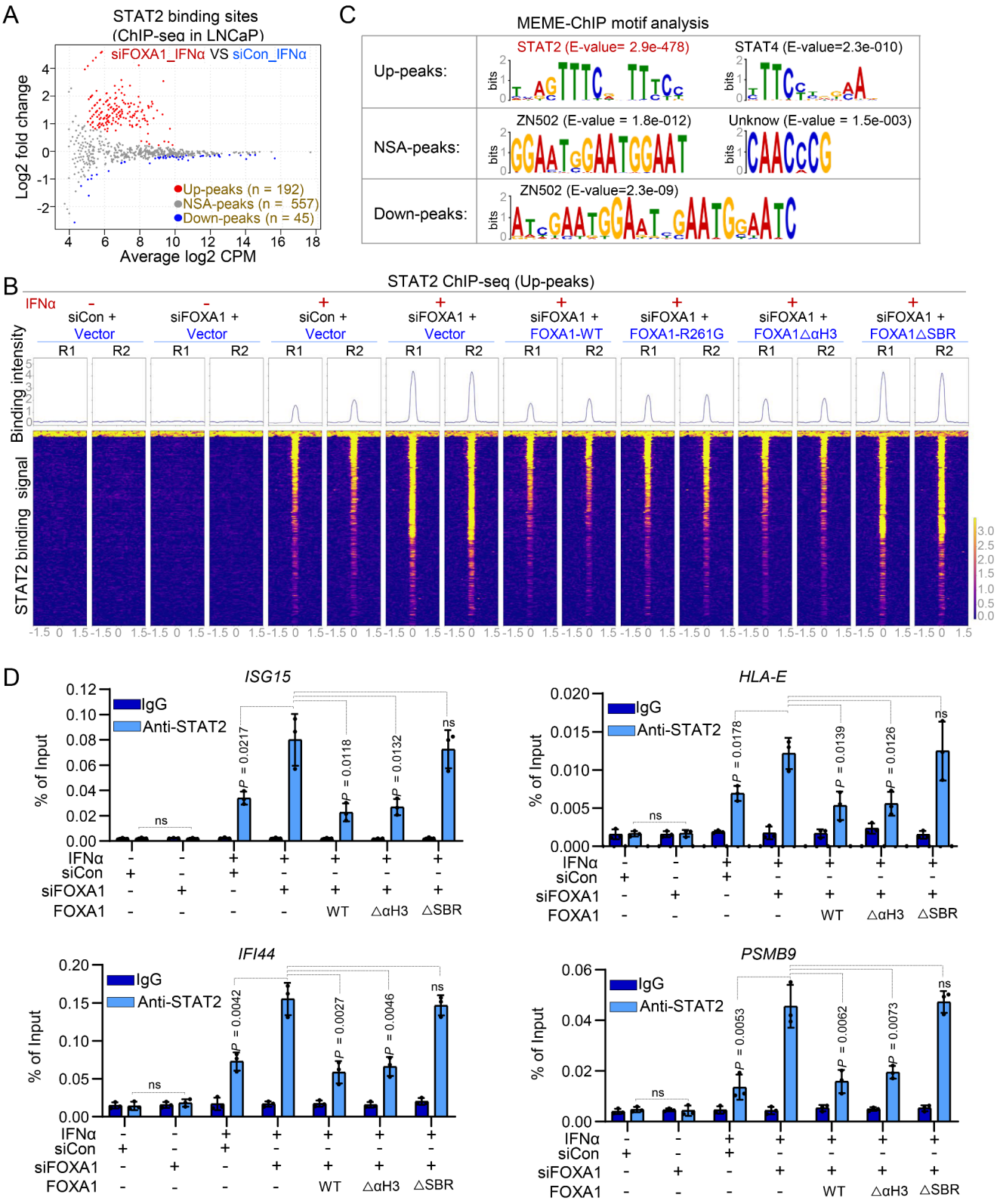

Figure 3. The effect of FOXA1 on STAT2 cistrome in PCa cells. (**A**) MA plot of STAT2 ChIP-seq data in LNCaP cells transfected with control or FOXA1-specific siRNAs in the presence or absence of IFNα treatment. Red dots (Up-peaks) and blue dots (Down-peaks) represent increased and decreased peaks (FDR < 0.05), respectively and gray dots indicate peaks with no significant alterations (NSA) (FDR > 0.05) after FOXA1 KD. (**B**) Heatmaps show the signaling intensity of 192 STAT2 ChIP-seq Up-peaks in LNCaP cells under the indicated cellular conditions. (**C**) MEME-ChIP DNA motif analysis in 192 STAT2 ChIP-seq Up-peaks, 557 NSA-peaks and 45 Down-peaks caused by FOXA1 KD in LNCaP cells. (**D**) ChIP-qPCR analysis of STAT2 occupancy at genomic loci of STAT2 target genes *ISG15*, *IFI44*, *HLA-E* and *PSMB9* under the indicated cellular conditions. Data shown as means ±SD (n = 3). Statistical significance was determined by one-way ANOVA with Bonferroni correction for multiple tests.

Figure 4

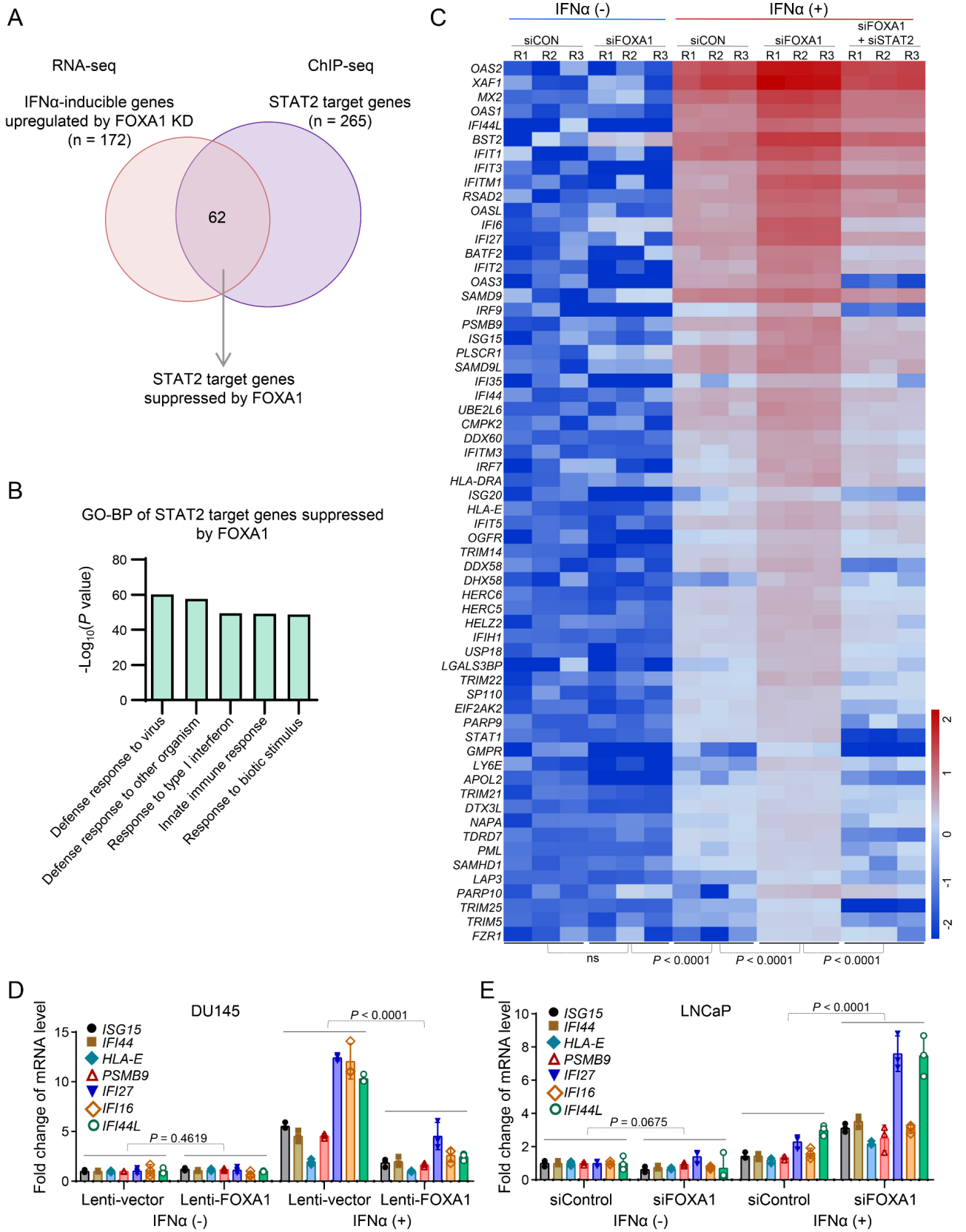

Figure 4. Identification of IFNα response genes suppressed by FOXA1. (**A**) Venn diagrams showing the overlap of IFNα-stimulated genes upregulated by FOXA1 KD with the STAT2 target genes identified by STAT2 ChIP-seq. (**B**) GO-BP pathway analysis of the 62 STAT2 target genes suppressed by FOXA1. (**C**) Heatmap shows the differential expression of the 62 STAT2 target genes suppressed by FOXA1 in LNCaP cells under the indicated cellular conditions. (**D** and **E**) RT-qPCR analysis of expression of STAT2 target genes *ISG15*, *IFI44*, *HLA-E*, *PSMB9, IFI27, IFI16* and *IFI44L* in FOXA1-negative DU145 cells infected with lentivirus expressing vector or FOXA1 (**D**) and in FOXA1-high LNCaP cells transfected control or FOXA1-specific siRNAs (**E**). Data shown as means ± SD (n = 3). Statistical significance was determined by one-way analysis of variance (ANOVA).

Figure 5

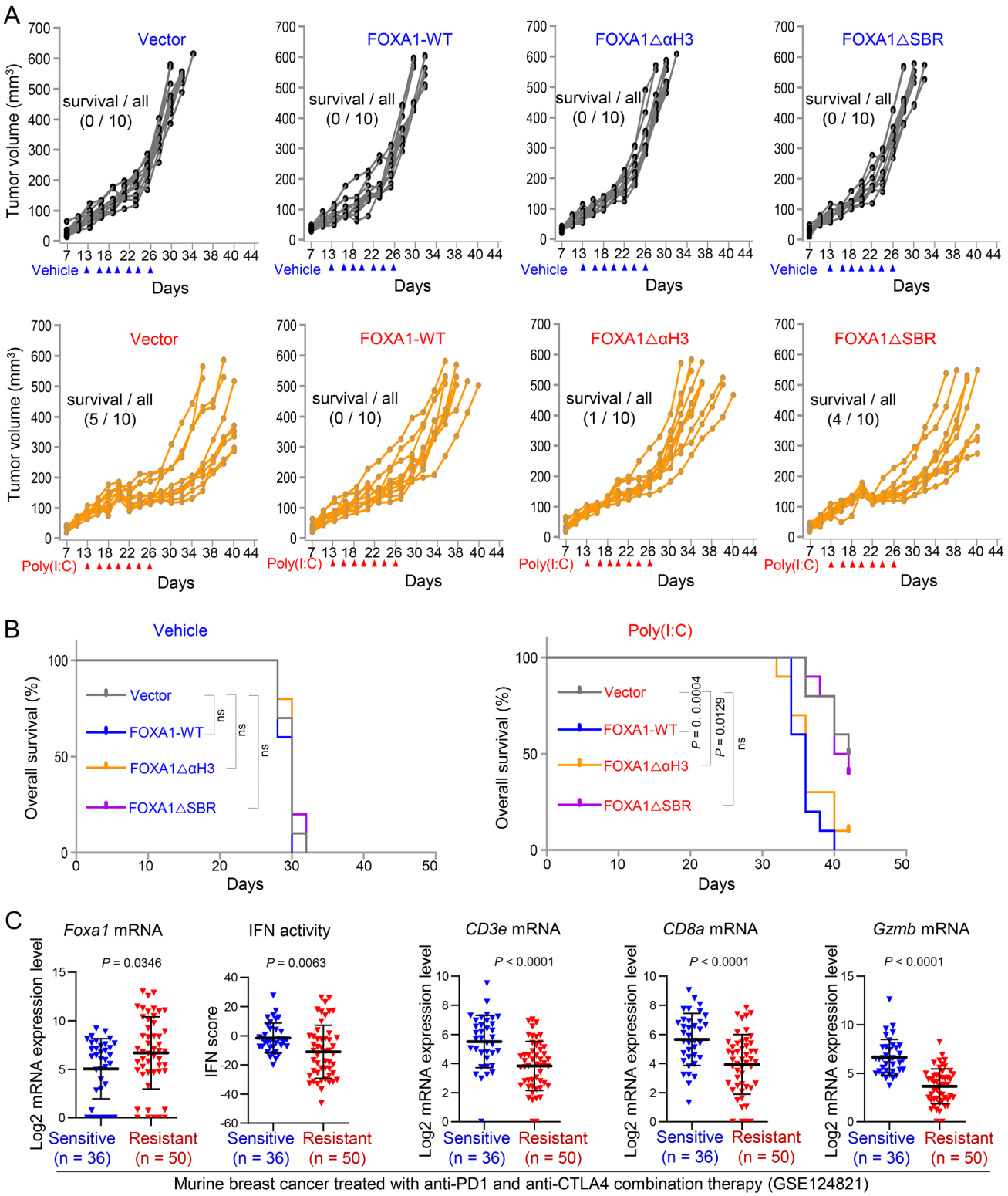

Figure 5. FOXA1 overexpression suppresses PCa immune response in mice. (**A**) Growth of TRAMP-C2 prostate tumors stably expressing vector, FOXA1-WT, FOXA1ΔαH3 or FOXA1ΔSBR treated with vehicle or Poly(I:C) at the indicated time points (arrowheads) in C57BL/6 mice. (**B**) Tumor-free survival of syngeneic mice bearing TRAMP-C2 tumors stably expressing vector, FOXA1-WT, FOXA1ΔαH3 or FOXA1ΔSBR treated with vehicle or Poly(I:C). Statistical significance was determined by Log-rank (Mantel-Cox) test. (**C**) Analysis of RNA-seq data from a cohort of murine BCa (GSE124821) showing the association of high expression of Foxa1 and low expression of IFN response genes (IFN activity) and *CD3e*, *CD8a* and *Gzmb* T cell marker genes with the responsiveness to anti-PD1 and anti-CTLA-4 combination therapy (resistant versus sensitive). Statistical comparison was done using Mann-Whitney U test.

Figure 6

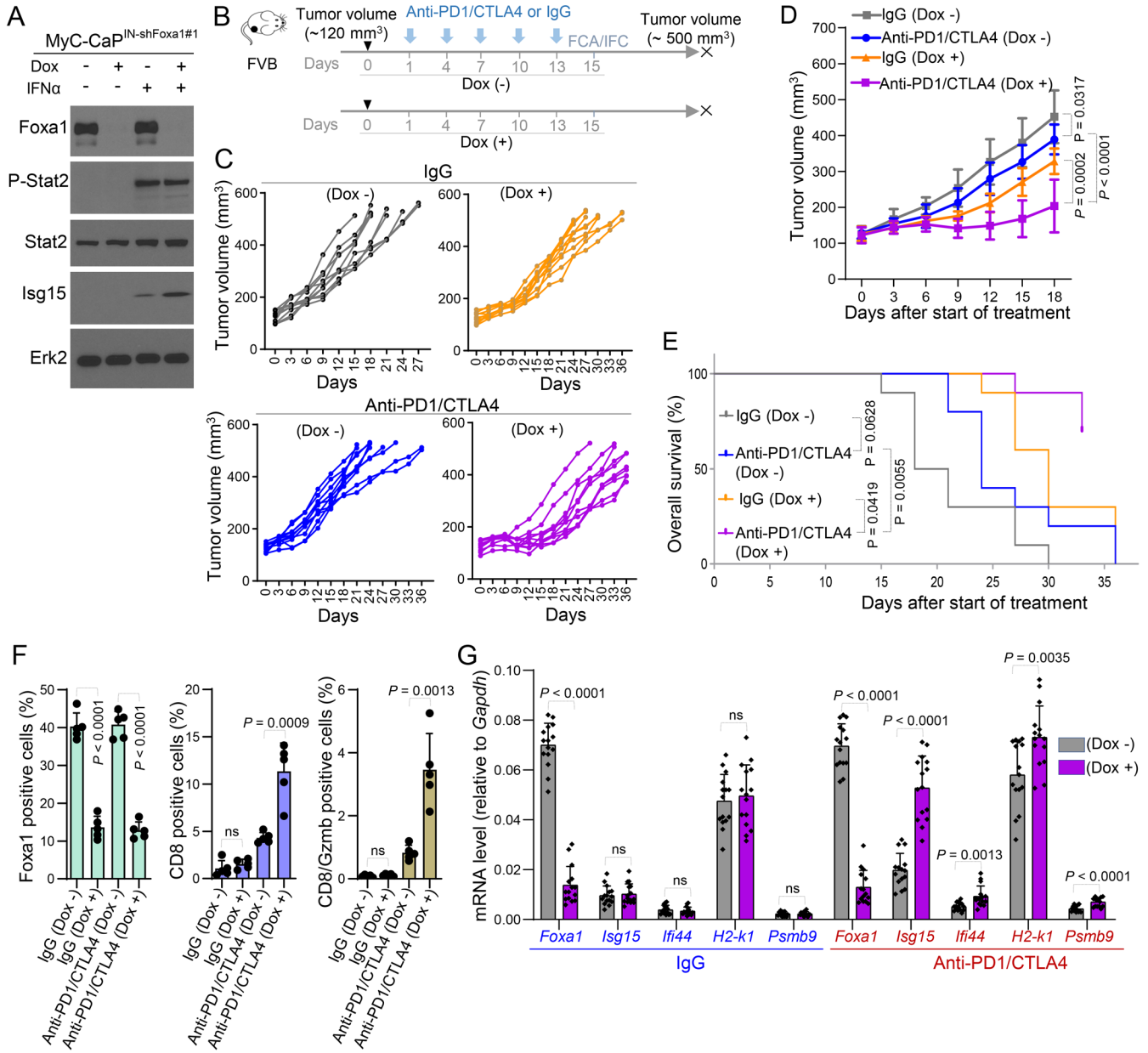

Figure 6. Foxa1 knockdown sensitizes murine PCa to anti-PD1 and anti-CTLA-4 combination therapy. (**A**) Western blot analysis of indicated proteins in MyC-CaP murine PCa cells stably expressing doxycycline-inducible lentiviral shFoxa1#1 (MyC-CaP$^{IN\text{-}shFoxa1\#1}$) and treated with or without doxycycline (Dox) or/and IFNα. Erk2, a loading control. (**B**) Schematic diagram of generation and anti-PD1/CTLA-4 treatment of MyC-CaP$^{IN\text{-}shFoxa1\#1}$ prostate tumors in syngeneic mice. Dox (-), without doxycycline treatment; Dox (+), with doxycycline treatment; FCA, Flow cytometry analysis; IFC, Immunofluorescent cytochemistry. (**C** and **D**) Growth of MyC-CaP$^{IN\text{-}shFoxa1\#1}$ prostate tumors treated with IgG or combination of anti-PD1/CTLA-4 at the indicated time points (arrowheads) in FVB mice (n = 10 mice/group). Statistical significance was determined by two-way analysis of variance (ANOVA). (**E**) Tumor-free survival of syngeneic mice bearing MyC-CaP$^{IN\text{-}shFoxa1\#1}$ prostate tumors treated with IgG or anti-PD1/CTLA-4 (n = 10 mice/group). Statistical significance was determined by Log-rank (Mantel-Cox) test. (**F**) Flow cytometry analysis of Foxa1, CD8 and Gzmb positive cells in MyC-CaP$^{IN\text{-}shFoxa1\#1}$ tumors from mice at two days after the last administration of IgG or anti-PD1/CTLA-4. Data were are shown in the bar graphs as means ± SD (n = 5 mice/group). Statistical significance was determined by one-way ANOVA with Bonferroni correction for multiple tests. (**G**) RT-qPCR analysis of *Foxa1* and murine Stat2 target genes *Isg15*, *Ifi44*, *H2-k1* and *Psmb9* in MyC-CaP$^{IN\text{-}shFoxa1\#1}$ tumors from mice at two days after the last administration of IgG or anti-PD1/CTLA-4. The data are presented as the mean± SD (n = 5 mice/group). Statistical significance was determined by one-way ANOVA with Bonferroni correction for multiple tests .

Figure 7

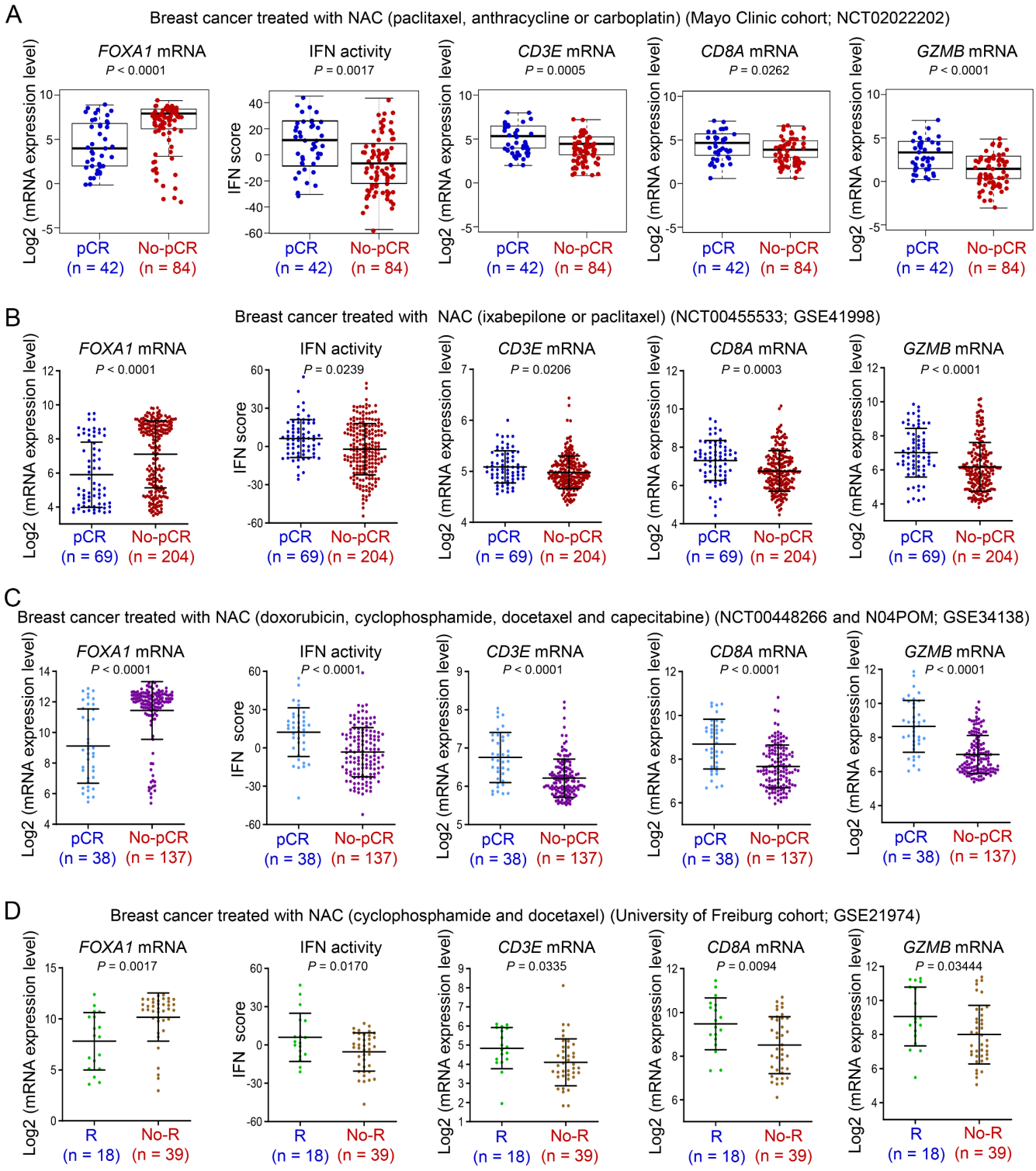

Figure 7. FOXA1 overexpression associates with resistance of neo-adjuvant chemotherapy (NAC) in cancer. (**A-C**) Analysis of RNA-seq data from a cohort of 126 BCa patients at Mayo Clinic (**A**) and microarray data from two independent cohorts of BCa (GSE41998 and GSE34138) (**B** and **C**) showing the association of high expression of *FOXA1* and low expression of IFN response genes (IFN activity) and *CD3E*, *CD8A* and *GZMB* T cell marker genes with the responsiveness to NAC (No-pCR versus pCR). pCR, pathological complete response; No-pCR, no pathological complete response. Statistical comparison was done using Mann-Whitney U test. (**D**) Analysis of microarray data from a cohort of BCa (GSE21974) showing the association of high expression of *FOXA1* and low expression of IFN response genes (IFN activity) and *CD3E*, *CD8A* and *GZMB* T cell marker genes with the responsiveness to NAC (No-R versus R). R, response; No-R, no response. Statistical comparison was done using Mann-Whitney U test.

Figure 8

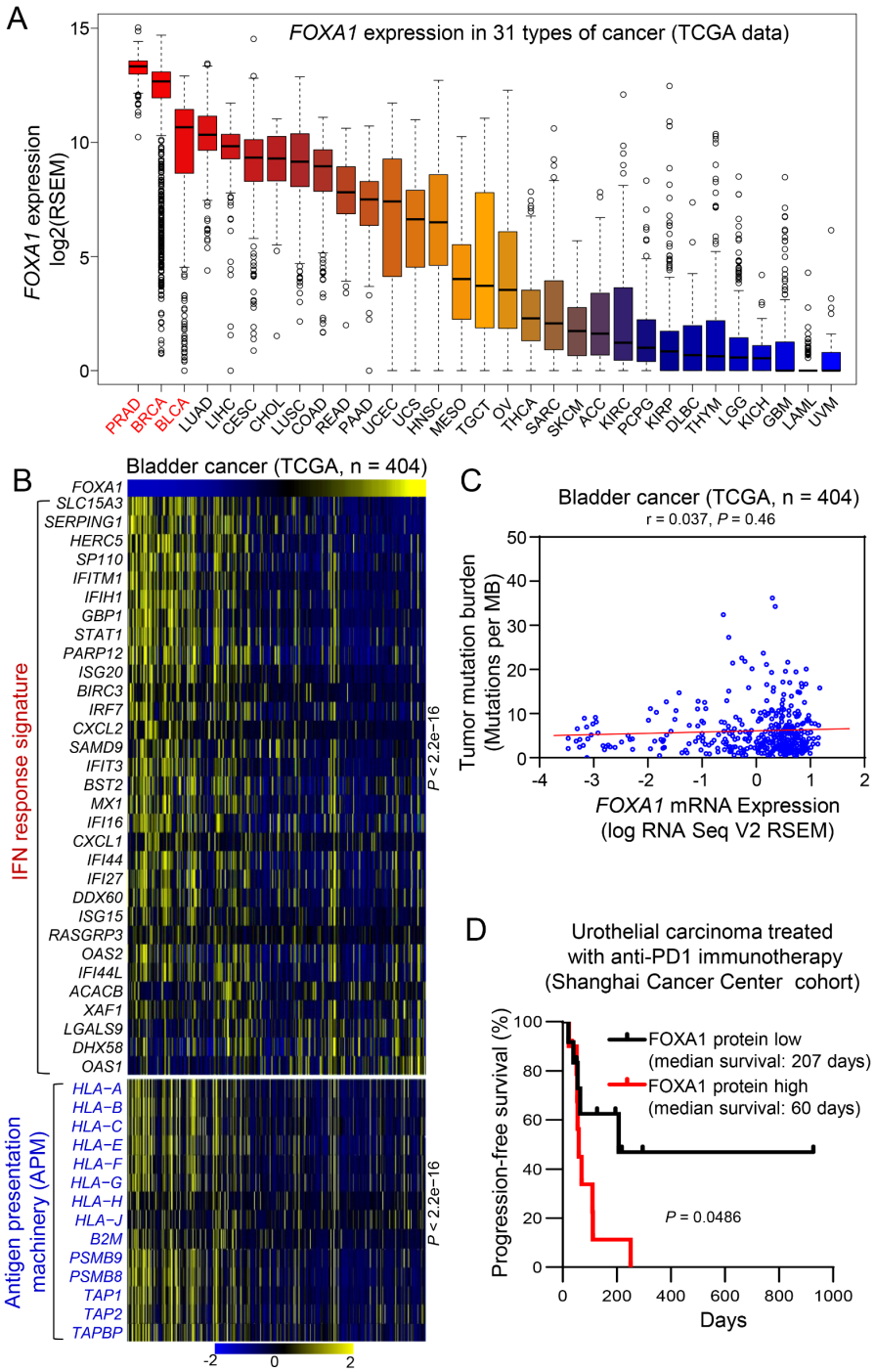

Figure 8. FOXA1 confers to immunotherapy resistance in bladder cancer. (**A**) Comparison of *FOXA1* mRNA level among 31 cancer types in the TCGA database, including PRAD (prostate adenocarcinoma), BRCA (breast invasive carcinoma), BLCA (bladder urothelial carcinoma), LUAD (lung adenocarcinoma), LIHC (liver hepatocellular carcinoma), CESC (cervical squamous cell carcinoma and endocervical adenocarcinoma), CHOL (cholangiocarcinoma), LUSC (lung squamous cell carcinoma), COAD (colon adenocarcinoma), READ (rectum adenocarcinoma), PAAD (pancreatic adenocarcinoma), UCEC (uterine corpus endometrial carcinoma), UCS (uterine carcinosarcoma), HNSC (head and neck squamous cell carcinoma), MESO (mesothelioma), TGCT (testicular germ cell tumors), OV (ovarian serous cystadenocarcinoma), THCA (thyroid carcinoma), SARC (sarcoma), SKCM (skin cutaneous melanoma), ACC (adrenocortical carcinoma), KIRC (kidney renal clear cell carcinoma), PCPG (pheochromocytoma and paraganglioma), KIRP (kidney renal papillary cell carcinoma), DLBC (lymphoid neoplasm diffuse large B-cell lymphoma), THYM (thymoma), LGG (brain lower grade glioma), KICH (kidney chromophobe), GBM (glioblastoma multiforme), LAML (acute myeloid leukemia) and UVM (uveal melanoma). (**B**) Heatmaps show the negative correlation of FOXA1 expression with the expression levels of IFN response signature genes and APM genes in the TCGA cohort of bladder cancers. Samples are ranked based on FOXA1 transcript levels. Statistical significance was determined by Pearson correlation test. (**C**) The correlation between FOXA1 level and TMB in the TCGA cohort of bladder cancers. Statistical significance was determined by Pearson correlation test. (**D**) Progression-free survival of patients with FOXA1-low or -high urothelial carcinomas treated with anti-PD1 immunotherapy. Statistical significance was determined by Log-rank (Mantel-Cox) test. Also see Supplementary Figure 18 and Supplementary Table 3 for FOXA1 IHC staining and patient's clinic information, respectively.

Figure 9

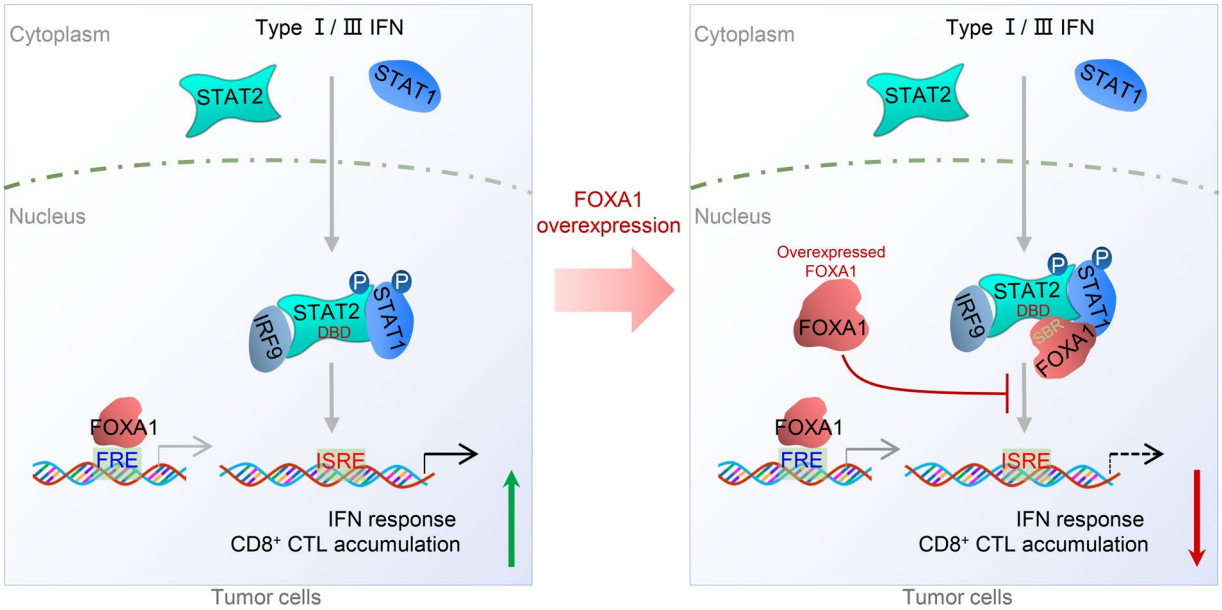

Figure 9. A hypothetical model deciphering FOXA1 overexpression-mediated suppression of IFN signaling and cancer immune response. Upon stimulation of cells with type I/III IFNs, STAT1 and STAT2 proteins become phosphorylated, dimerized (STAT2/STAT1 heterodimer) and translocate into nucleus to initiate the transcription of interferon-stimulated genes (ISGs) by binding to ISRE and ultimately promote cancer immune response (**Left**). However, in FOXA1-overexpressing tumor cells, the overexpressed FOXA1 protein, in a manner independent of its binding of DNA on chromatin, inhibits the DNA accessibility of STAT protein complex and impairs ISG expression, thereby suppressing cancer immune response (**Right**). IFN, Interferon; FRE, forkhead response element; ISRE, interferon stimulation response element; CTL, cytotoxic T lymphocyte; DBD, DNA binding domain; SBR, STAT2 binding region; P, phosphorylation.